Supplemental Information

High Thermoelectric Conversion through an Optimal Contribution of Electronic Carriers in Polymeric Mixed Ionic-electronic Conducting Films

*Cheolhyun Cho, Byeonggwan Kim, Sienoh Park and Eunkyoung Kim**

Contents

Experimental section

Materials

Poly(2-acrylamido-2-methyl-1-propanesulfonic acid) solution (PAMPS, weight average molecular weight = 2,000,000, 15 wt% in water), Potassium ferricyanide(III), Acetaldehyde, 5-(4-dimethylaminobenzylidene)rhodamine and Silver nitrate were purchased from Sigma Aldrich. Graphene Flakes (GF) with a thickness of 1.6 nm and fewer than 3 layers of graphene were purchased from Graphene Supermarket (graphene nanopowder AO-1). Deionized (DI) water (Extra Pure) was purchased from Duksan General Science. Cerasolzer #186 (indium wire) was purchased from Kuroda Electric Co. LTD. The chemicals were used in the experiment without further treatment. Indium tin oxide (ITO) glass (13 Ω $\square^{-1}$) was purchased from Wooyang GMS Co., Ltd.

Synthesis of PFG solution

PAMPS (15 wt% in DI water) was added to DI water diluted to 4.9 wt%. And the GF was added to the PAMPS solution at a concentration of 1, 2, 3, 5, 7, 10 and 15 solid wt%, then the mixture was ultrasonicated at 0 °C for 60 min to be dispersed. The mixture was stored in a vial under magnetic stirring. Potassium ferricyanide (5 mM) was added to the stored mixture solution, and the mixture was stirred at the room temperature for 2 h. Next, Acetaldehyde (60 mM) was added to the mixture, and the mixture was stirred at the room temperature for 1h to obtain PFG1, PFG2, PFG3, PFG5, PFG7, PFG10 and PFG15, respectively.

Synthesis of Prussian blue analogs (PBAs) solution

PAMPS (15 wt% in DI water) was added to DI water diluted to 4.9 wt%. Potassium ferrocyanide / Potassium ferricyanide (5 mM) or $FeCl_3$ (5 mM) were added to the PAMPS solution, and the mixture was stirred at the room temperature for 2 h. Next, Acetaldehyde (60 mM) was added to the mixture, and the mixture was stirred at the room temperature for 1 h to obtain Sample2-6 solution. Using the solution of Sample2-6 solution, the TE films were prepared same as the film fabrication method previously described and TE measurement was conducted under the ΔT of 5.3 K and 80% RH. After the Sample1 (PFG0) was synthesized, green-colored

soluble BG was produced (Figure S4). The Sample 2 showed a darker green color under an environment where the BG could be better generated due to the addition of $FeCl_3$. However, the mechanism of BG production with $FeCl_3$ actually inhibited the production of free cyanide, showing a lower negative *S* (-23.0 mV K^{-1}). The Sample 4 in which the PB was produced by the reaction with potassium ferrocyanide and $FeCl_3$ showed a dark blue color, while the Sample 3, in which $FeCl_3$ was not added, showed a light blue color. In the mechanism that generates PB, very low *S* was generated because it did not supply thermos-diffusive carriers. Even in Sample 4, TE phenomenon was not observed because too much PB blocked the movement of ions. In Sample 7 (PFG3), as emphasized several times in the manuscript, GF was well-dispersed and a black solution without precipitate was observed.

Film fabrication

Two of Au electrode lines (thickness: 100 nm, width: 1 mm, length: 2 cm, and distance between electrodes: 3 mm) were deposited on top of a clean polyethylene terephthalate film (PET, thickness: 0.5 mm) by thermal evaporation under a high vacuum (5×10^{-6} Pa) through a stainless steel shadow mask. The Au-deposited PET film was cut to a size of 0.5 × 3 cm^2, and an area of 0.5 × 0.5 cm^2 was treated with O_3 plasma for 5 min. The PFG solution (30 μL) was drop-casted on the O_3 plasma-treated active area and dried at room temperature and 50% relative humidity (RH) for 2 h. The thickness of the PFG films was measured using a Bruker Surface Profiler (DektakXT) at various RH levels. Flat surface of the PFG film was formed by well-dispersed graphene flakes in the composite and the control of the solution volume to drop-casted area. The optimized PFG3 film was uniformly coated with a thickness of 130 μm and 80% RH.

Transparent and electrically conductive ITO glasses were used as electrodes for the vertically structured PFG3 film. A spacer with an area of 1 × 1 cm^2 and a thickness of 3 mm was made using polyimide (PI) tape. The PFG solution (2.8 ml) was continuously filled into the spacer and dried for 10 days. Finally, the PFG3 film with a thickness of 3 mm at 80% RH was completely sealed using another ITO glass.

Fabrication of TE modules

A PET film (thickness: 0.5 mm) with 20 legs of the Au electrode (thickness: 100 nm, width: 2 mm, and distance between electrodes: 5 mm) was prepared using the same process as described above. An area of 2 × 7 mm^2

of each leg was treated with O_3 plasma for 5 min using a stainless mask exposing an active area. The PFG3 solution (10 μL) was drop-casted on each leg and dried at room temperature for 40 min. The dried module was stored in a chamber at 80% RH.

Fabrication of various MIEC films

1) PFG0//GF

The graphene flakes (GF) dispersed DI water solution (5.9 mg/mL) was dispersed using the ultrasonicator. The Au-deposited PET film was cut to a size of 0.5 × 3 cm^2, and an area of 0.5 × 0.5 cm^2 was treated with O_3 plasma for 5 min. The graphene flakes (GF) dispersed DI water solution (30 μL) was drop-casted on the O_3 plasma-treated active area and dried at room temperature and 50% RH for 4 h. After the drop-casted film was completely dried, the PFG0 solution (30 μL) was drop-casted on the GF-PET film and dried at room temperature and 50% RH for 2 h to make bi-layer film which contains same amount of GFs with the PFG3 film.

2) PFG0//PGF10

The Au-deposited PET film was cut to a size of 0.5 × 3 cm^2, and an area of 0.5 × 0.5 cm^2 was treated with O_3 plasma for 5 min. The PFG10 solution (9 μL) was drop-casted on the O_3 plasma-treated active area and dried at room temperature and 50% RH for 1 h. After the drop-casted film was completely dried, the PFG0 solution (21 μL) was drop-casted on the PFG10-PET film and dried at room temperature and 50% RH for 2 h to produce bi-layer film which contains same amount of GFs with the PFG3 film.

3) PFG3_MD

The PFG3_MD solution was prepared with the same process except for the dispersion process using mechanically stirring instead of ultrasonication. The Au-deposited PET film was cut to a size of 0.5 × 3 cm^2, and an area of 0.5 × 0.5 cm^2 was treated with O_3 plasma for 5 min. The PFG3_MD solution (30 μL) was drop-casted on the O_3 plasma-treated active area and dried at room temperature and 50% RH for 2 h. Rough surface of the PFG film was formed by undispersed GFs in the composite.

Supplemental note

HCN titration experiment

Treatment to inhibit the production of HCN in an acidic environment is necessary. Acetaldehyde was added to completely remove HCN present in very small amounts from Equation (S1-3).[1]

$$PAMPSO_3H + CN^- \rightarrow PAMPSO_3^- + HCN$$

Equation (S1)

$$PAMPSO_3H + HCN + CH_3C(=O)H + 2H_2O \rightarrow PAMPSO_3^- + CH_3CH(OH)C(=O)OH + NH_4^+$$

Equation (S2)

Quenching Overall,

$$2PAMPSO_3H + CN^- + CH_3C(=O)H + 2H_2O \rightarrow 2PAMPSO_3^- + CH_3CH(OH)C(=O)OH + NH_4^+$$

Equation (S3)

Lactonitrile produced by the addition of acetaldehyde was converted to lactic acid under slightly acidic condition, helping to make the removal of HCN irreversible. Removal of HCN and generation of NH_4^+ were verified through the HCN titration experiment and TOF-SIMS analysis.

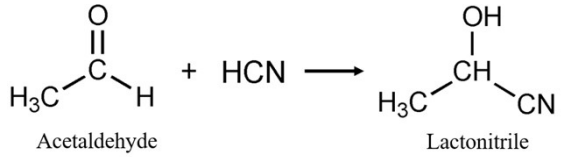

Acetaldehyde Lactonitrile

Equation (S4)

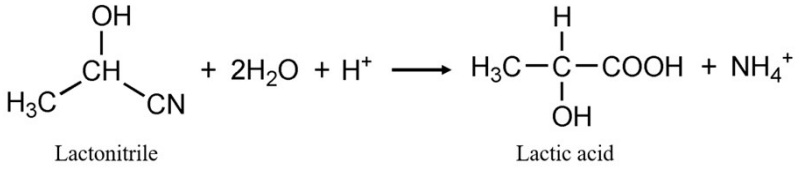

Lactonitrile Lactic acid

Equation (S5)

5-(4-dimethylaminobenzylidene)rhodamine (0.76 mM) dissolved in acetone and $AgNO_3$ (10 mM) dissolved in DI water were prepared for HCN titration. PFG3 solution (20 μL) and 5-(4-dimethylaminobenzylidene)rhodamine solution (200 μL) were added to 10 g of DI water. At this 5-(4-dimethylaminobenzylidene)rhodamine-based aqueous solution, 20 μL of PFG0UA (Fig. S2b), PFG0 (Fig. S2c), PFG3 (Fig. S2d) were added. In Fig. S2a, the maximum FL intensity decreased and a broad peak was formed at 400~500 nm as $AgNO_3$ solution was added. After 10 μL of $AgNO_3$ solution was added, the maximum FL peak was fixed at 410 nm which is shifted from 405 nm, showing an almost identical graph and maintaining the color of the solution. When $AgNO_3$ solution was added to the diluted mixture of PFG0UA, $AgNO_3$ reacted with HCN formed in the PFG0 solution in a 1:1 equivalent. When 18 μL of $AgNO_3$ solution was added, the color of the solution remains the same. In contrast,

in the mixture containing PFG0 and PFG3 solution, the color remains the same and the maximum FL peak was no longer shifted when 10 μl of $AgNO_3$ solution was added, same as in Fig. S2a. (Fig. S2c,d) Through this titration experiment, it was demonstrated quantitatively that acetaldehyde removed toxic HCN that may remain in the solution.

XPS analysis

The composition of the PFG specimen was determined by X-ray photoelectron spectroscopy (XPS) analysis, which was conducted for finding the ratio of Fe^{2+} and Fe^{3+} for a composition of BG (Fig. S5). The Fe 2p spectra was deconvoluted into 6 peaks, which included $2p_{2/3}$ (709 and 711 eV), Satellite (714.7 and 718.8 eV), and $2p_{1/2}$ (722.6 and 724.6 eV) of Fe^{2+} and Fe^{3+}.[2] By comparing the sum of the integrated areas of the $2p_{3/2}$ and $2p_{1/2}$ peaks corresponding to Fe^{2+} and Fe^{3+} in PFG-0, -3, -10, the composition ratio of Fe^{2+} and Fe^{3+} was determined. In the PFG-0, -3, -10, Fe^{2+}/Fe^{3+} of the BGs were 0.29, 0.33 and 0.31, respectively, which correspond to x = 0.3, 0.33 and 0.31 of $[KFe^{II}Fe^{III}(CN)_6]_x[Fe^{III}Fe^{III}(CN)_6]_{1-x}$, respectively.

Characterization

The hydrodynamic radius (R_h) of PFG0~10 in suspension were measured using dynamic light scattering (DLS) spectra with a Zetasizer Nano ZS90 (Malvern Instruments, inc.). Then, 20 μL of a PFG solution was mixed with 35 mL of deionized water for dilution. A supernatant solution was used for the DLS measurement after 0 h and 24 h. Error bars reflect the standard deviation from ten identical measurements.

Grazing-incidence wide-angle X-ray scattering (GIWAXS) patterns were collected at the 3C beam line in the Pohang Accelerator Laboratory (PAL) using a monochromatized 10.032 keV (λ= 0.12358 nm) X-ray irradiation source with a two-dimensional charge-coupled device detector (Rayonix 2D MAR165). The scattering vector (q) was calculated from the equation (q=4π·sin(θ)/λ). Each thin film was prepared by casting the solution (120 μL) onto a SiO_2/Si substrate (1×1 cm^2). The same amount of graphene flakes and potassium ferricyanide contained in the PFG3 solution were dispersed in the DI water and then casted.

UV-vis-NIR spectra of the PAMPS, PAMPS-Graphene3 (PG3), PFG0 and PFG3 films (thickness: 15 μm) were measured by Lambda 750, UV/Vis/NIR Spectrophotometer, PerkinElmer. In order to advantageously

analyze the absorbance of dark-colored films, the solution volume was adjusted so that each film was spread thinly on a glass slide.

Raman spectrum of PAMPS, graphene flakes and PFG films was obtained using a Raman spectroscopy (LabRAM Aramis, HORIBA) using a 532 nm laser. Each solution was drop-casted on a glass slide and dried at room temperature. The graphene flakes were measured at the solid state. The area and thickness of the films were the same with the films used for TE measurement.

Transmission electron microscopy (TEM) images, TEM-EDS images, and electron diffraction patterns were obtained by JEM-F200, JEOL Korea Ltd. The PFG films were stored at 80% RH and then cryogenically cut perpendicular to the film using Ultramicrotome, RMC. Cross sections of films cut in the vertical direction were observed.

Time-of-flight secondary ion mass spectrum (TOF-SIMS) analysis was performed using an ION-TOF V instrument. A 30 keV Bi3 primary beam was used as a primary ion current source (0.675 pA). First, the PFG sample on PET film was prepared by applying a ΔT of 5.3 K and 80% RH for 1000 s over an area of 2 × 1 cm2. To prevent further diffusion, once the temperature differential was removed, the film was immediately cut into two parts from the central part of the film (1 × 1 cm2) and analyzed to assess anion distribution changes due to thermo-diffusion. This ensured the ionic composition of the hot and cold parts remained distinct, as ion diffusion is a slow process. It takes approximately several hundred seconds for ions to reach the peak redistribution under the applied conditions, and their movement during the cutting process is negligible. Thus, the difference in ion intensity observed at the center of the film via TOF-SIMS accurately reflects the thermo-diffusion induced redistribution rather than post-cutting diffusion. PAMPS, PFG0UA and PFG sample on PET film (1 × 1 cm2) were prepared for the observation of HCN removal. The central regions (300 × 300 μm2) were examined under identical sputtering conditions (2 min), and atomic composition counts were determined by integrating each peak.

The cyclic voltammetry (CV) of the PAMPS and PFG films were measured by universal potentiostat (model CHI 624B, CH Instruments, Inc.). All films were stored in the same sealed chamber with the same humidity level and measured at a scan rate of 50 mV s^{-1}.

The thermovoltage (Vout) of the PFG films was measured by a homemade setup with Keithley 2182A Nanovoltmeter (or Keithley 6514 Electrometer). The thermal current output (Iout) of the PFG films was measured directly using Keithley 6485 picoammeter, without the need for an external load. Two Peltier devices

attached to an aluminum heat sink using a thermal paste (~4 mm apart) generated the temperature gradient. The temperature gradient was set by applying various input currents (+0.7 to −0.7 A), on the two Peltier devices using a Keithley 2400 Multimeter. The temperature difference in the samples was checked by using a high-resolution IR camera (FLIR E40) in a dark room at room temperature (23~26 °C with an error of 0.2 °C). The humidity during the V_{out} measurement was controlled by the volume of deionized water in the sealed chamber. The RH was measured by a hygrometer (sensitivity of 1% RH). The V_{out} of the TE device was measured after saturation of a specific humidity (1 h) and stabilization of the voltage signal. For storage stability measurement, the film was kept in the ambient condition at 50% RH, and after a specific time past, the V_{out} measurement was repeated at 80% RH, ΔT of 5.3 K, and RT conditions. The I measurement was performed in the same condition. For the PTE experiment, the NIR coherent diode laser (1064 nm, 0−1.0 W, 3-Laser Technology) was irradiated perpendicularly to the one leg of PFG3 film (15 cm apart), and the laser beam was collimated to generate a beam area of 2 × 3.5 mm^2. The temperature gradient and time-drive temperature change of the films were obtained using the IR camera and control programmed software in a thermally stabilized dark room at room temperature, which was set to 23-25 °C with an error of 0.2 °C, for clear analysis. For the in- situ PT tracing experiment, the PET film with a size of 2.5 × 2.5 cm^2 was treated with O_3 plasma for 5 min. The PFG3 solution (750 μL) was drop-casted on the O_3 plasma-treated active area and dried at room temperature and 50% RH for 6 h. The dried film was stored in a chamber at 80% RH. The PEDOT:Tos film on the PET substrate was fabricated using the same recipe for PEDOT:Tos (P5) film.[3] The NIR laser head (1064 nm) was handy-controlled to irradiate the surface of the PTE film with sufficient humidity. On the surface of the PTE film, the temperature profile when the laser irradiated point was moved was recorded by an IR camera (Supplemental video). For the solar-PTE experiment, the artificial sunlight of 1 sun power (100 mW cm^2) supplied by a solar simulator (Sun2000, ABET Tech.) was irradiated perpendicularly on the one leg (2 × 5 mm^2) of the PFG3 film, of which the rest is covered by a mask. The distance between the aluminum mask and the PFG3 film was adjusted so that the swelled film by humidity did not touch. The solar-PTE experiment for PTE module with 20 legs was performed in the same condition. In that case, stainless mask covered by aluminum foil was used so that the sunlight could reach each leg (2 × 2 mm^2). The measurement for observing the temperature gradient and time-drive temperature change of the film and the PTE module was performed in the same condition using the IR camera. The solar-PTE experiment for the vertically structured PFG3 film was also performed. The vertical TE device was placed on a heat sink and exposed to the sunlight without a mask.

The electrochemical impedance spectroscopy (EIS) was performed using an electrochemical interface and impedance analyzer (COMPACTSTAT, IVIUM technology). The samples (area of 5 mm × 5 mm) were measured by 2-electrode setup at room temperature and different RH levels. Normally, the EIS was measured in-plane direction through the film on substrate with Au electrodes. The EIS spectrum was fit using the equivalent circuit mode (Fig. S11) and the simulated parameters were summarized in Table S4.

The Hall measurements were conducted using an HMS-5300 (Ecopia) system. The applied current ranged from 1 mA to 10 mA, with increments of 1 mA per step, and a magnetic field of 0.556 T was applied during the measurements. The films used for Hall measurements were prepared using the same fabrication method as the PFG films on PET film substrates, with the exception that no Au electrodes were included in these films. This setup ensures that the Hall measurement accurately reflects the intrinsic properties of the PFG films, free from any influence of the Au electrodes

The thermal conductivity (κ) was calculated from the equation $\kappa = C_p\ \alpha\ \rho$, where C_p is the specific heat capacitance, α is the thermal diffusivity, and ρ is the density of the sample. The C_p was measured from differential scanning calorimetry (DSC, 200 F3 Maia, NETZSCH) under N_2 gas flow at a heating rate of 10 °C min^{-1}. The in-plane α was measured by laser flash analysis (LFA457, NETZCH) at a 25 °C chamber and 40% RH. PFG composite solution was drop-casted into a rectangular shaped Teflon mold and dried at room temperature for 48 h to obtain a thickness of 0.5 mm. To calculate density of films (ρ_{film}) at various humidity levels (50-90% RH), the mass of the films at different RH level was measured. According to the Equation (S6), the volumetric change by water absorption is originated from different swelling efficiency of hydrogel network with respect to the change of RH level. V_{film} and m_{film} are the volume and mass of the film measured at 40% RH as an initial value. V_{total} is calculated as the product of area and thickness of the film.

$$V_{total}(RH) = V_{film}(RH) + V_{water}(RH)$$

$$= m_{film}(RH)/\rho_{film}(RH) + \Delta m_{water}/\rho_{water} \qquad \text{Equation (S6)}$$

$$\rho_{film}(RH) = \frac{m_{film}(RH)}{V_{total}(RH) - \Delta m_{water}/\rho_{water}} \qquad \text{Equation (S7)}$$

The weight of the samples at different RH level was measured for the sample stored in the chamber of corresponding humidity prior to use. Δm_{water} was calculated from the change in mass of the film between a

particular RH level and 40% RH. The water density (ρ_{water}) of 0.997 g cm^{-3} was used for the calculation. Therefore, the ρ_{film}(RH) was calculated from Equation (S7).

The κ of the PFG samples at various humidity levels (50−90% RH) was calculated from the Equation (S8).

$$\kappa = \kappa_p \emptyset_p + \kappa_w \emptyset_w \quad \text{Equation (S8)}$$

where ø is volume fraction. The subscripts p and w corresponded to the PFG sample at 40% RH and water, respectively. The κ_w of 0.6 W m^{-1} K^{-1} was used for the calculation.

The σ was calculated from Equation (S9)

$$\sigma = \frac{d}{RA} \quad \text{Equation (S9)}$$

where σ is ionic conductivity (σ_i) or electrical conductivity (σ_e), d is the distance between electrodes, R is Z_i or Z_e obtained from the EIS analysis, and A is the area penetrated by thermo-diffusive carriers.

The capacitance (C) of TE films was calculated from the Equation (S10).

$$C = \frac{\int I dV}{v \times A \times \Delta V} \quad \text{Equation (S10)}$$

Where I is the voltammetric current, v is the voltage scan rate, A is the active area of the TE film, and ΔV is the applied voltage.

The electrochemical energy storage E_{ch} of the TE module was calculated from the Equation (S11).[4]

$$E_{ch} = \frac{1}{2} C (S\Delta T)^2 \quad \text{Equation (S11)}$$

where C is the capacitor (in here 1 mF), S is the Seebeck coefficient (total), and ΔT is the temperature gradient across the two electrodes (in here 5.3 K).

Energy density (E, J m^{-2}) and power density (P, W m^{-2}) of the TE module was calculated from the Equation (S12-13).

$$E = \frac{E_{ch}}{A} \quad \text{Equation (S12)}$$

$$P = \frac{V_{out} I_{out}}{A} \quad \text{Equation (S13)}$$

where E_{ch} is the electrochemical energy storage calculated using the capacitor (in here 1 mF) and the ΔT (in here 4.9 K), A is the total area of the legs of the module, V_{out} is the thermovoltage, and I_{out} is the output current.

The maximum charging efficiency of ionic thermoelectric supercapacitor (η_{iTE}) was calculated from the Equation (S15).

$$\eta_{iTE} = \frac{\Delta T}{T_H} \frac{ZT_i}{2ZT_i + \frac{10T}{T_H} - \frac{1}{2}ZT_i\frac{\Delta T}{T_H}} \quad \text{Equation (S15)}$$

where T_H is the temperature at hot part, ZT is the figure of merit, and T is the absolute temperature on thermoelectric measurement. The η_{iTE} for organic ionic thermoelectric materials in Table S6 and Figure S23a was determined from Equation (S15).

The maximum thermoelectric efficiency (η_{max}) of conventional thermoelectric materials was calculated from the Equation (S16).

$$\eta_{max} = \frac{\Delta T}{T_H} \frac{\sqrt{1+ZT}-1}{\sqrt{1+ZT}+\frac{T_C}{T_H}} \quad \text{Equation (S16)}$$

where T_C is the temperature at cold part and ZT is the figure of merit. The η_{max} for inorganic thermoelectric materials in Table S6 and Figure S23a was determined from Equation (S16).

The PT conversion efficiency (η_{PT}) of the PT materials was calculated from the Equation (S17).

$$\eta_{PT} = \frac{ha(T_{max} - T_{surr}) - Q_{sub}}{I_0(1 - 10^{-A_\lambda})} \quad \text{Equation (S17)}$$

Where h is the heat-transfer coefficient, a is the surface area of the film, T_{max} is the maximum equilibrium temperature of the film, T_{surr} is the ambient temperature of the surroundings, Q_{sub} is the heat dissipated from light absorbed by the substrate without the sample film, I_0 is the laser power, and A_λ is the laser wavelength. T_{surr} was 25 °C. 1064 nm (24.8 mW) was irradiated on the film. Q_{sub} was measured independently using a pure PET film without a PFG layer. However, the temperature change by the NIR laser (1064 nm, 24.8 mW) was almost undetectable (< 0.1 K).

Supplemental tables

Table S1. d(*q*y) and d(*q*z) of SiO_2, graphene flakes, and PFG films with various graphene flake concentrations obtained by GIWAXS analysis

Sample	d(*q*y) (Å)				d(*q*z) (Å)			
SiO_2	4.22				4.19			
Graphene flakes	3.57				3.58			
Potassium ferricyanide	6.75	4.18	3.89	3.22	4.33	4.16	3.19	
PFG0	6.83	4.28	4.16	3.22	6.12	3.21	3.14	
PFG3	12.82	6.41	4.83		10.65		4.72	
PFG5	12.32	6.48	5.15	4.76	10.47	5.03	4.65	
PFG7	12.32	6.54	5.28	4.76	10.65	5.07	4.69	3.67
PFG10	12.57	6.48	5.15	4.65	10.65	5.15	4.62	3.53
PFG12	12.32	6.68	5.19	4.76	10.83	5.15	4.65	3.55
PFG15	12.57	6.54	5.28	4.8	10.83	5.15	4.69	3.59

.

Sample	V_{ox}[a] (V)	V_{red}[b] (V)	Peak-to-peak Separation (V)	Capacitance (mF cm^{-2})
PAMPS	0.32	0.32	0.67	0.012
PFG0	-0.24, 0.19	-0.21, 0.25	0.03, 0.06	0.16
PFG2	0.12	-0.26	0.38	0.49
PFG3	0.28	-0.27	0.55	1.22
PFG5	0.39	-0.38	0.77	1.94
PFG7	0.48	-0.5	0.98	2.76
PFG10				1.67
PFG12				1.94
PFG15				1.61
PG3	0.11	-0.1	0.21	1.18

Table S2. Electrochemical properties of PAMPS and the PFG films with various graphene flake concentrations.

Hot plate T (°C)	I^a (A)	T^b (°C)	ΔT^c (K)	S (mV K^{-1})
-[d]	2-0.2, -0.7 / +0.3	29.7	6.9	-27.0
-[d]	-0.5 / +0.5	25.0	5.3	-40.8
36	-0.5 / +0.5	29.7	6.9	-34.0
40	-0.5 / +0.5	34.5	7.4	-26.8
45	-0.5 / +0.5	40.2	7.8	-22.5
55	-0.5 / +0.5	48.3	8.1	-17.7

All the measurements were performed at a scan rate of 50 mV s^{-1} using cyclic voltammetry. [a] Peaks for oxidation voltage. [b] Peaks for reduction voltage.

Table S3. Temperature environments for TE measurements and TE properties of the PFG3 film.

[a] Applied current to Peltier devices. [b] Temperature of the environment for the TE measurement. [C] Temperature difference in hot and cold regions of the PFG3 film. [d] Hot plate was turned off. All the TE measurements were performed at 80% RH.

Table S4. Summary of simulated impedance parameters obtained by fitting the electrochemical impedance spectroscopy results.

Sample	RH (%)	C_{geo}[a] (F)	CPE-T[b]	CPE-P[c]	Z_i (Ohm)[d]	Z_e (Ohm)[e]
PAMPS	80	1.84E-10	1.15E-06	0.88	465	629290
PG3	80	1.64E-10	6.40E-05	0.44	578	30153
PFG0	50	4.46E-11	1.87E-06	0.93	2516	46689
	60	8.85E-11	2.72E-06	0.99	997	16232
	70	1.17E-10	3.31E-06	0.95	689	7686
	80	1.54E-10	3.54E-06	0.92	503	4305
PFG2	50	7.04E-11	9.12E-05	0.74	2204	17609
	60	1.04E-10	1.50E-05	0.78	1205	5798
	70	1.38E-10	1.47E-05	0.78	778	4405
	80	1.77E-10	1.53E-05	0.75	590	2101
PFG3	50	1.12E-10	8.45E-06	0.57	1635	8074
	60	1.15E-10	4.38E-05	0.47	1134	2389
	70	1.37E-10	1.60E-05	0.77	1048	1876
	80	1.79E-10	1.73E-05	0.78	640	1497
	90	2.25E-10	7.36E-05	0.66	352	1572
PFG5	50	9.07E-11	1.34E-06	0.51	2851	11345
	60	1.03E-10	5.60E-04	0.49	4093	2135
	70	1.26E-10	4.10E-04	0.39	1940	1718
	80	1.69E-10	4.70E-04	0.38	1050	1273
PFG7	50	1.08E-10	1.41E-07	0.72	2087	10676
	60	1.29E-10	1.60E-03	0.41	2779	1619
	70	1.54E-10	1.30E-03	0.61	1742	1248
	80	1.93E-10	1.30E-03	0.6	1176	932
PFG10	50	1.64E-10	2.90E-07	0.69	2684	1212
	60	2.00E-10	3.71E-07	0.66	1507	1267
	70	2.41E-10	2.45E-06	0.53	997	1212
	80	2.20E-10	3.60E-04	0.57	994	844.5
PFG0//GF	80	1.48E-10	4.47E-06	0.82	584	2622
PFG0//PFG10	80	1.54E-10	1.52E-05	0.67	607	2862
PFG3_MD	80	5.79E-07	2.59E-06	0.43	1881	231340

[a] Geometrical capacitance. [b,c] Constant phase element. CPE-T is related to pseudo capacitance. CPE-P is related to the semi-circle in the Nyquist plot. [d] Ionic and [e] electronic impedance calculated for the films from the simulated electrochemical impedance spectrum in Figure S11.

Sample	Major carrier, type[a]	RH (%)	S_i[b] (mV K^{-1})	S_e[c] (mV K^{-1})	Total S[d] (mV K^{-1})	I_{out}[e] (μA)	σ_i[f] (S m^{-1})	σ_e[g] (S m^{-1})	PF[h] (mW m^{-1} K^{-2})	PF_e[i] (mW m^{-1} K^{-2})	K[j] (W m^{-1} K^{-2})	ZT[k]	Capacitance (mF cm^{-2})	Power density (mW m^{-2})	Energy density (J m^{-2})
PAMPS	I, p	80	24.5		24.5		9.5	0.007	5.72	5.70	0.333	4.2	0.012		
PG3	M, p	80					7.7	0.15		0			1.18		
PFG0	M, n	50					3.1	0.17		0	0.279				
		60					6.5	0.4		0	0.296				
		70					8.1	0.72		0	0.327				
		80	-33.9		-33.9	-0.26	10.3	1.2	11.9	11.8	0.372	8.7	0.16	0.37	24.8
PFG2	M, n	50					3.4	0.43		0	0.389				
		60					5.2	1.1		0	0.402				
		70					7	1.2		0	0.422				
		80	-41.5		-41.5	-1.95	8.5	2.4	14.6	14.6	0.449	10.	0.49	12.7	
PFG3	M, n	50	-11.5	-0.07	-11.6		4.4	0.88	0.59	0.582	0.492	0.4			
		60	-21.9	-0.41	-22.3		5.4	2.6	2.68	2.59	0.5	1.9			
		70	-26.8	-0.69	-27.5		5	2.8	3.76	3.59	0.512	2.7			
		80	-39.8	-0.99	-40.8	-2.98	7.2	3.1	12.0	11.4	0.529	8.8	1.22	18.6	36.0
		90	-41.5		-41.5		11.3	2.5	19.6	19.5	0.54	14.			
PFG5	M, n	50	-4.5	-0.25	-4.75		2.4	0.6	0.055	0.0486	0.389	0.0			
		60	-9.8	-0.12	-9.92		2.8	1.4	0.27	0.269	0.407	0.1			
		70	-15.7	-0.29	-15.9		2.6	2.9	0.66	0.641	0.432	0.4			
		80	-27.2	-0.44	-27.6	-3.62	4.2	3.4	3.18	3.11	0.463	2.3	1.94	11.9	
PFG7	M, n	50	-2.5	0.04	-2.4		3.1	0.6	0.018	0.0194					
		60	-4.7	-0.09	-4.8		3.3	1.9	0.077	0.0729					
		70	-10.6	-0.12	-10.7		2.7	3.8	0.31	0.303					
		80	-21.5	-0.23	-21.7	-3.97	3.6	4.5	1.69	1.66			2.76	6.4	10.2
PFG10	M, n	50	-0.06	0.02	-0.04		2.6	5.8	3×10^{-6}	9.36×10^{-6}	0.326				
		60	-0.34	0.03	-0.31		3.9	4.7	4×10^{-4}	4.51×10^{-4}	0.339				
		70	-0.58	0.05	-0.53		5.2	4.3	0.002	1.75×10^{-3}	0.358				
		80	-2.1	0.04	-2.06	-3.7	4.5	5.3	0.019	0.0198	0.382	0.0	1.67	0.44	
PFG12	E, p	50	0	0.04	0.04			17.6							
	M, n	80	-1.32	0.05	-1.27			4.93							
PFG15	E, p	50	0	0.034	0.034			30.1							
	M, p	80	-0.019	0.044	0.025			7.16							
PFG3_MD	M, n	80			-11.7		2.45	0.02							
PFG0//GF	M, n	80			-2.26		7.9	1.76							
PFG0//PFG1	M, n	80			-0.47		6.84	1.41							

Table S5. TE parameters of the PFG films.

[a] Major carrier, where M represents mixed ionic-electronic conductor, I represents ionic conductor and E represents electrical conductor. [b] Seebeck coefficient generated by the Soret effect at a ΔT of 5.3 K. [c] Seebeck coefficient generated by the Seebeck effect at a ΔT of 5.3 K. The values of S_i and S_e are V_i and V_e divided by a ΔT of 5.3 K. [d] Sum of S_i and S_e. [e] Output current where a ΔT of 5.3 K was applied. [f] Ionic conductivity. [g] Electrical conductivity [h] Power factor [i] Electronic power factor [j] Thermal conductivity. [k] Figure-of-merit.

Sample	Major carrier, type[a]	T^b (K)	ΔT^c (K)	σ_i^d (S m^{-1})	σ_e^e (S m^{-1})	S^f (mV K^{-1})	PF^g (mW m^{-1} K^{-2})	κ^h (W m^{-1} K^{-2})	ZT^i	Power density (mW m^{-2})	Energy density (J m^{-2})	η^j (%)	Ref
PFG3	M, n	298	5.3	7.2	3.1	-40.8	12.0	0.52	8.8	18.6	36.0	0.56	This work
NPP65	M, n	298	4.8	15.9	0.008	-25.0	9.94	0.41	7.2	0.21	8.8	0.48	5
PEDOT:PSS+ $CuCl_2$	M, n	298	4.5	5.26	0.3	-18.2	1.74	0.34	1.53	0.38	0.78	0.18	6
PEDOT:PSS:PSSH	M, p	298	5	29.1	0.03	16.2	7.64	0.5	4.51	1.62	2.24	0.40	7
EMIM:DCA/SWNT/SDS	M, p	296	0.5	0.094	6×10^{-6}	23	0.05	0.273	0.054			9×10^{-4}	8
PANI:PAAMPSA:PA/SiO_2	I, p	298		18.7		17.9	5.99	0.477	3.74	0.024	0.019	0.129	9
PVDF–HFP /EMIM:DCA	I, p	298	0.6	0.67		26.1	0.455	0.176	0.75			0.013	10
EMIM:DCA/SiO_2	I, p	298	4	4.75		14.8	1.04	0.21	1.47	0.16	0.32	0.152	11
PEDOT:Tos	E, p	298	6.9		94000	0.079	0.059			0.13			3
$Na_{0.03}Sn_{0.992}Se$	E, p	783	10[k]		11800	0.27	0.86	0.21	3.1			0.43	12
		300	10[k]		8500	0.19	0.29	0.65	0.13			0.10	12
$Bi_{0.48}Sb_{1.52}Te_3$	E, p	330	10[k]		55000	0.246	3.3	0.75	1.3			0.67	13
		300	10[k]		63700	0.236	3.5	0.80	1.4			0.68	13
$Pb_{0.98}Na_{0.02}Te$–SrTe 8%	E, p	923	10[k]		30000	0.295	2.61	1	2.4			0.32	14
		300	10[k]		209000	0.089	1.66	2.9	0.17			0.13	14
$PbTe_{0.7}S_{0.3}$– 2.5% K-doped	E, p	923	10[k]		16000	0.298	1.42	0.6	2.2			0.30	15
		300	10[k]		146000	0.071	0.74	1.56	0.14			0.11	15
SnSe (b axis)	E, p	923	10[k]		9000	0.33	0.98	0.35	2.6			0.33	16
		300	10[k]		1100	0.50	0.28	0.71	0.12			0.09	16
$Cu_{1.94}Al_{0.02}Se$	E, p	1029	10[k]		27500	0.249	1.7	0.67	2.6			0.30	17
		300	10[k]		170000	0.078	1.0	1.2	0.26			0.19	17
$(Cu_{0.78}Ag_{0.22})_2(Te_{0.78}S_{0.22})$	E, p	1000	10[k]		20000	0.225	1.0	0.52	2.0			0.26	18
		300	10[k]		46100	0.068	0.21	0.40	0.16			0.16	18
Te–PEDOT:PSS	E, p	400	6		7230	0.325	0.76	0.59	0.54			0.16	19
		300	6		4310	0.311	0.42	0.68	0.18			0.08	19
$Bi_2Te_{2.79}Se_{0.21}$ + 0.067 wt%	E, n	350	10[k]		99200	-0.21	4.4	1.1	1.4			0.61	20
		300	10[k]		121300	-0.20	4.8	1.11	1.3			0.66	20
$Bi_2Te_{2.79}Se_{0.21}$	E, n	357	10[k]		94000	-0.197	3.6	1.1	1.2			0.54	21
		300	10[k]		119000	-0.186	4.1	1.12	1.1			0.62	21

Table S6. TE parameters of the PFG film in comparison with other organic and inorganic TE materials reported in the previous literatures.

[a] Major carrier, where M represents mixed ionic-electronic conductor, I represents ionic conductor, and E represents electrical conductor. [b] Absolute temperature. [c] Temperature difference between hot and cold region. [d] Ionic conductivity. [e] Electrical conductivity. [f] Seebeck coefficient. [g] Power factor. [h] Thermal conductivity. [i] Figure-of-merit. [j] TE efficiency. Maximum charging efficiency for the iTE and mTE materials (η_{iTE}) and maximum TE efficiency (η_{max}) for inorganic TE materials. [k] A ΔT of 10 K was set for a low temperature gradient

Table S7. PTE parameters of the PFG film in comparison with other PTE materials reported in the previous literatures.

Sample	Major carrier, type[a]	Light Source (nm)	Light power (mw)	T^b (K)	ΔT^c (K)	$S_{PTE}{}^d$ (mV K^{-1})	σ^e (S m^{-1})	$PF_{PTE}{}^f$ (mW m^{-1} K^{-2})	κ^g (W m^{-1} K^{-2})	$ZT_{PTE}{}^h$	Power density (mW m^{-2})	$\eta_{PT}{}^i$ (%)	Ref
PFG2	M, n	1064	24.8	298	4.5	-40.5	8.5	13.9	0.449	10.2	12.2		This work
PFG3	M, n	1064	24.8	298	4.6	-39.8	7.2	11.4	0.529	8.4	17.9	89	This work
PFG5	M, n	1064	24.8	298	5.6	-23.2	4.2	2.24	0.463	1.6	9.9		This work
NPP65	M, n	800	22	298	1.4	-25.1	15.9	9.94	0.41	7.2	0.21		5
PEDOT:PSS/Te NW	E, p	320-2500		298	26	0.153		0.008	0.42	0.006	0.0046		22
CNT@s-Au	E, p	808		298	322	0.081					2.125		23
PBI/MWCNT	E, p	520	17.4	298	33	0.008	220.2	1.5×10^{-5}	0.41	1.1×10^{-5}	0.89		24
PEDOT:PSS/HCNT	E, p	808	1800	305	25.7						0.016		25
PEDOS-C6	E, p	808	780	298	30	0.03	33500	0.354				42.5	26
PTII	E, p	1700	17	296	11.7	0.28	2.2	0.0018				25.1	27
TzQI-TDPP	E, n	1700	17	296	14.4	-0.31	0.14	1.3×10^{-4}				30.9	27
EPG	E, p	1064	39.5	298	3.42	0.082	169000	1.15	1	0.35			28
PEDOT:Tos (P3)	E, p	808	191	298	102	0.076	114000	0.066				49	3
PEDOT:Tos (P4)	E, p	808	191	298	106	0.079	94000	0.059			0.13	54	3
PEDOT:Tos (P5)	E, p	808	191	298	99	0.08	92000	0.06				52	3
PEDOT:Tos (P9)	E, p	1064	220	298	143	5.3	0.037	2.47	3.4×10^{-6}			93	3

[a] Major carrier, where M represents mixed ionic-electronic conductor and E represents electrical conductor. [b] Absolute temperature. [c] Temperature difference between hot and cold region. [d] Seebeck coefficient by a PTE effect. [e] Major carrier conductivity. Ionic conductivity for the mTE materials and electrical conductivity for the eTE materials. [f] Power factor by a PTE effect. [g] Thermal conductivity. [h] Figure-of-merit by a PTE effect. [i] Photothermal conversion efficiency.

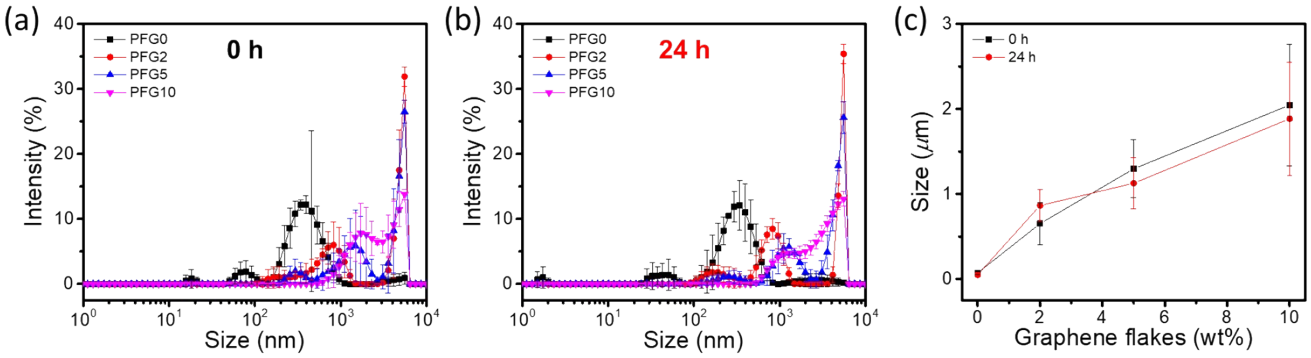

Supplemental figures

Figure S1. Size distribution of diluted PFG solutions by a dynamic laser scattering (DLS) measured after (a) 0 h and (b) 24 h. (c) Hydrodynamic radius (R_h) of dilute PFG0~10 microgels measured after 0 h and 24 h.

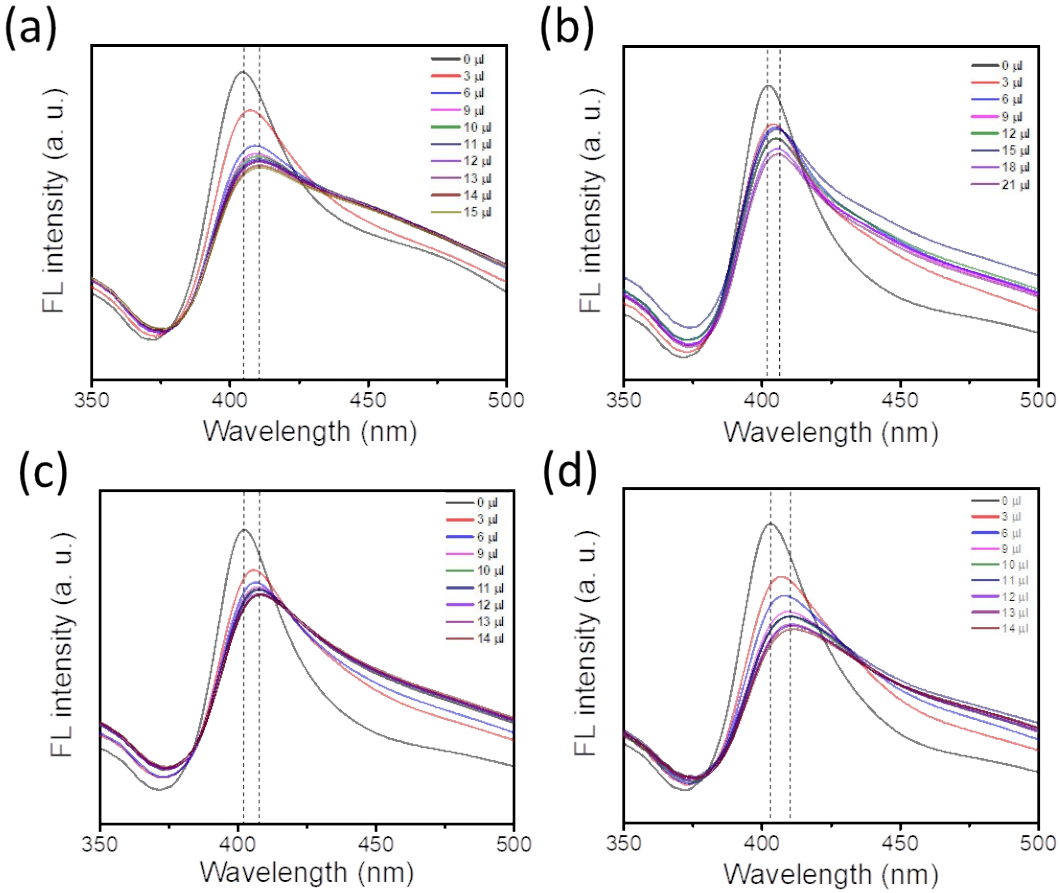

Figure S2. HCN titration experiment for the PFG solutions using 5-(4-dimethylaminobenzylidene)rhodamine (0.76 mM) dissolved in acetone and $AgNO_3$ (10 mM) dissolved in H_2O. Fluorescence spectra of the 5-(4-dimethylaminobenzylidene)rhodamine added (a) H_2O and diluted (b) PFG0UA, (c) PFG0, and (d) PFG3 in H_2O with the addition of $AgNO_3$ aqueous solution. For the redshift of λ_{max} ((a) 405 >> 410 nm, (b) 402 >> 407 nm, (c) 402 >> 408 nm, and (d) 403 >> 411 nm), 10, 18, 10, and 10 μL of $AgNO_3$ aqueous solution were added, respectively.

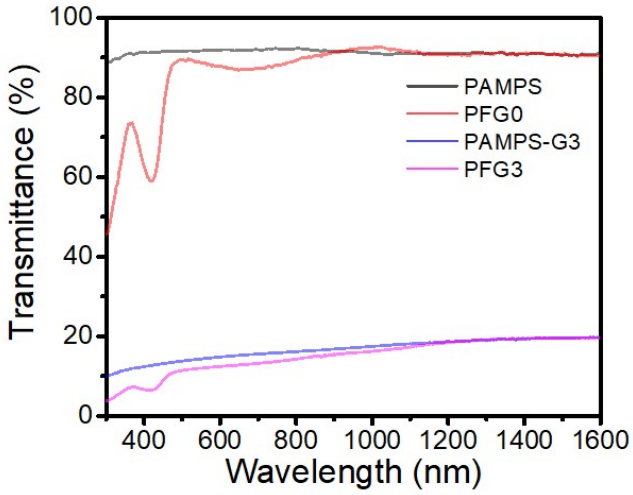

Figure S3. UV-Vis-NIR spectrum of the PAMPS, PG3, PFG0, and PFG3 films with the thickness of 15 μm on the glass slide.

Figure S4. Photographs of various Prussian blue analogs (PBAs). The number on the vials means below.

1) PAMPS + $K_3[Fe(CN)_6]$ (5 mM)

2) PAMPS + $K_3[Fe(CN)_6]$ (5 mM) + $FeCl_3$ (5 mM)

3) PAMPS + $K_4[Fe(CN)_6]$ (5 mM)

4) PAMPS + $K_4[Fe(CN)_6]$ (5 mM) + $FeCl_3$ (5 mM)

5) PAMPS + $K_3[Fe(CN)_6]$ (2.5 mM) + $K_4[Fe(CN)_6]$ (2.5 mM)

6) PAMPS + $FeCl_3$ (5 mM)

7) PAMPS + $K_3[Fe(CN)_6]$ (5 mM) + GF (3wt % to PAMPS)

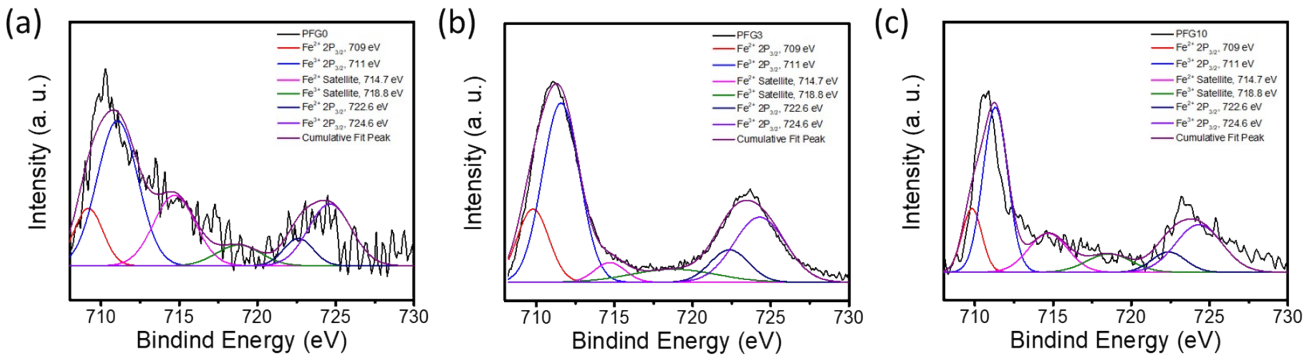

Figure S5. XPS spectra of (a) PFG0 (b) PFG3, and (c) PFG10 films including deconvoluted Fe 2p peaks.

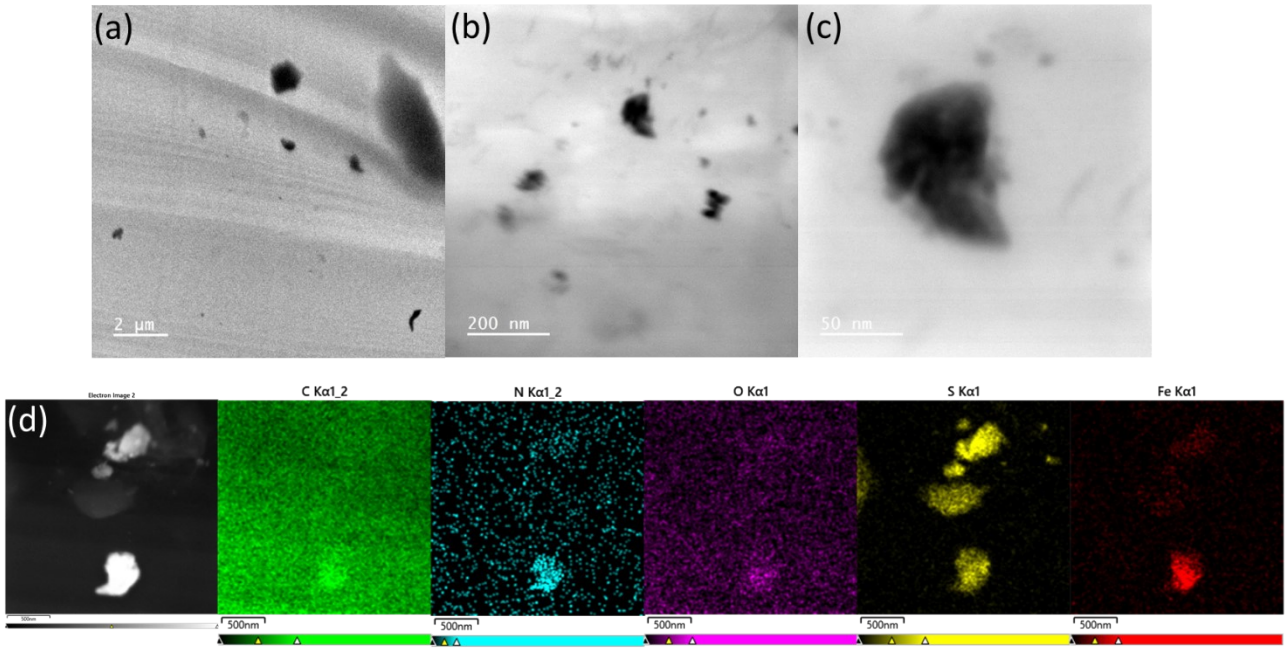

Figure S6. (a-c) TEM images of the PFG0 film obtained at various magnifications. (d) EDS images of the PFG0 film.

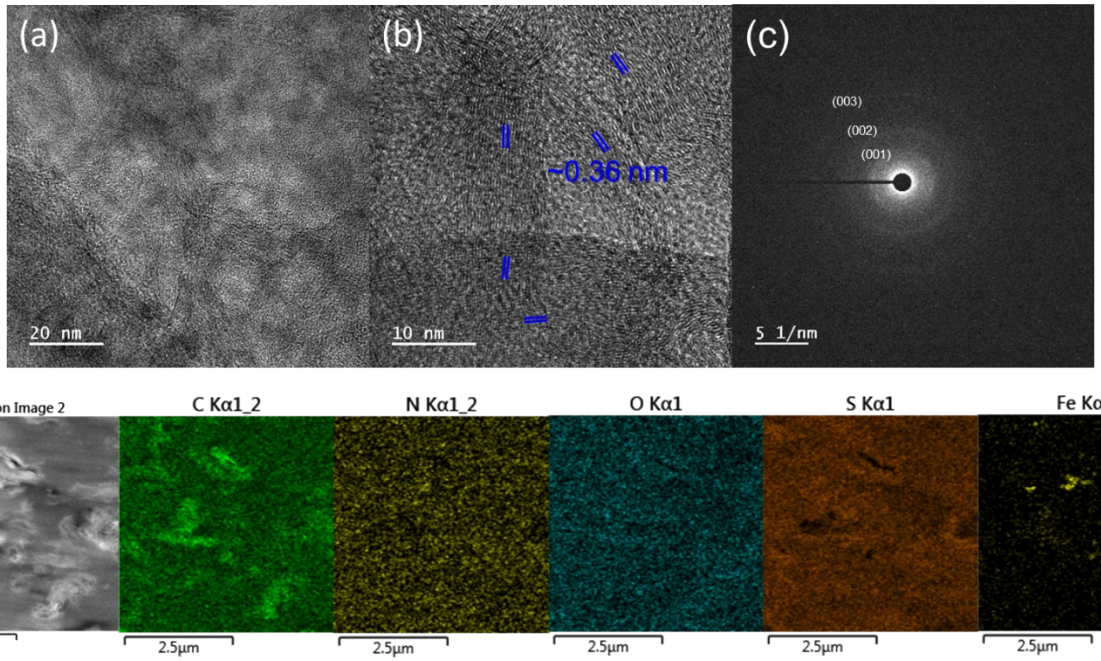

Figure S7. (a, b) TEM images of the PFG3 film obtained at various magnifications. (c) The electron diffraction pattern obtained from (b). (d) EDS images of the PFG3 film.

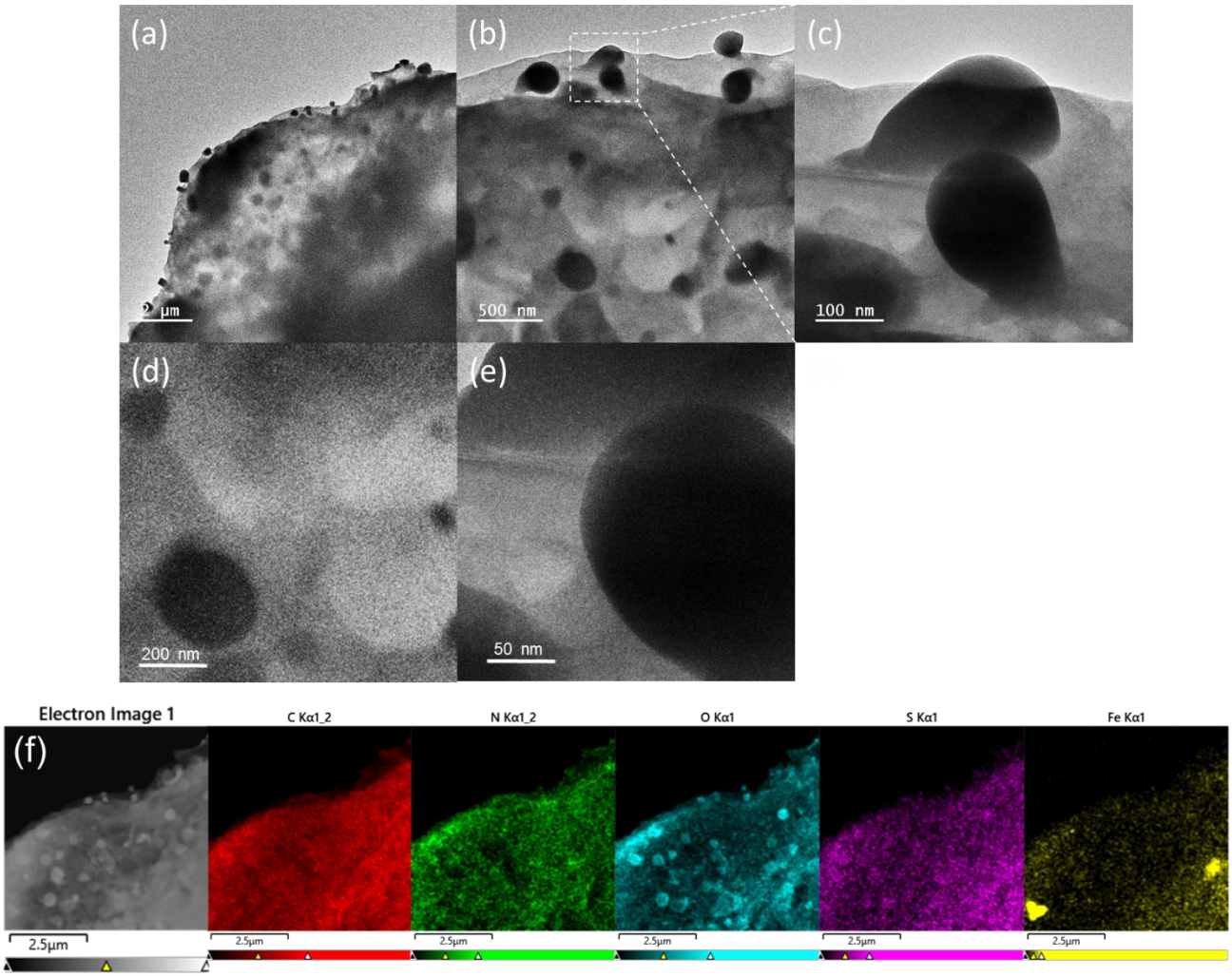

Figure S8. (a-e) TEM images of the PFG10 film obtained at various magnifications. The magnified image (c) obtained from (b). (f) EDS images of the PFG10 film.

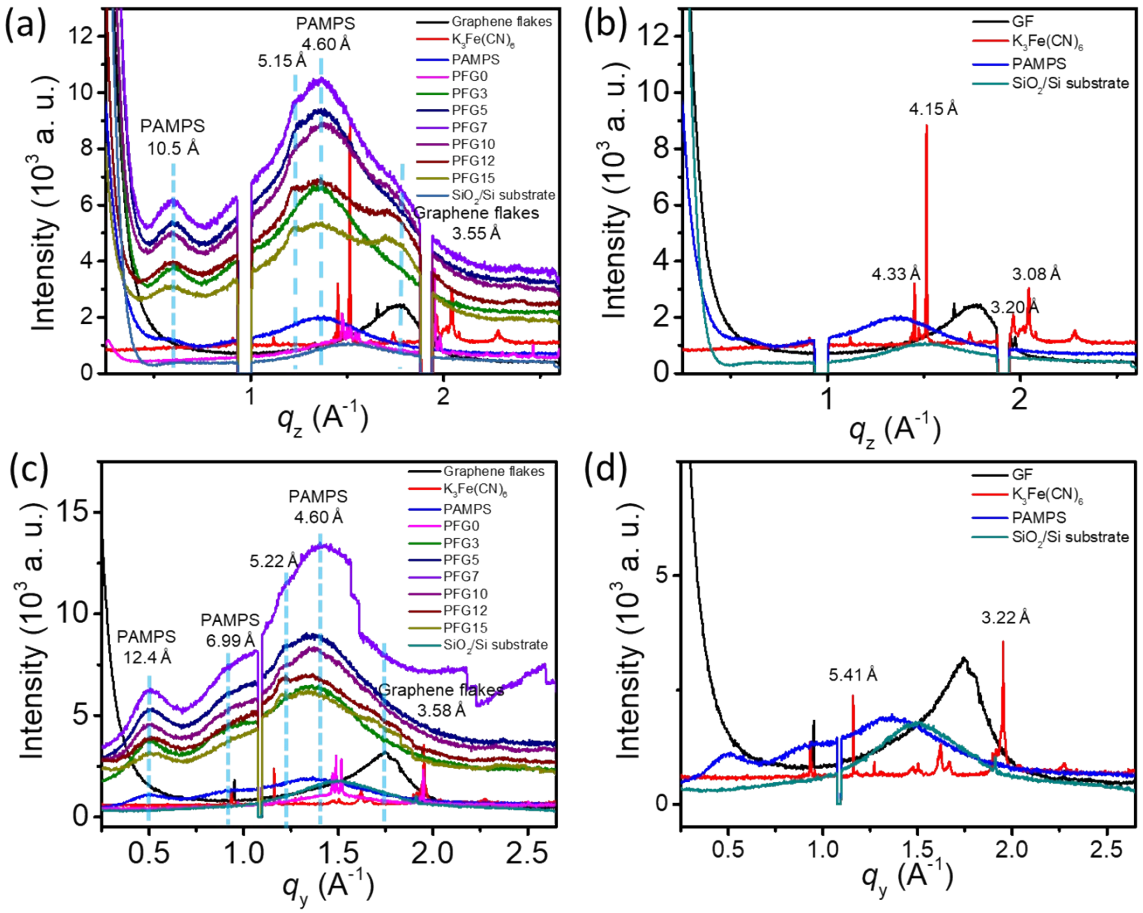

Figure S9. The (a, b) q_z and (c, d) q_y profiles of the 2D GIWAXS patterns of PFG-based films on the SiO_2/Si substrate.

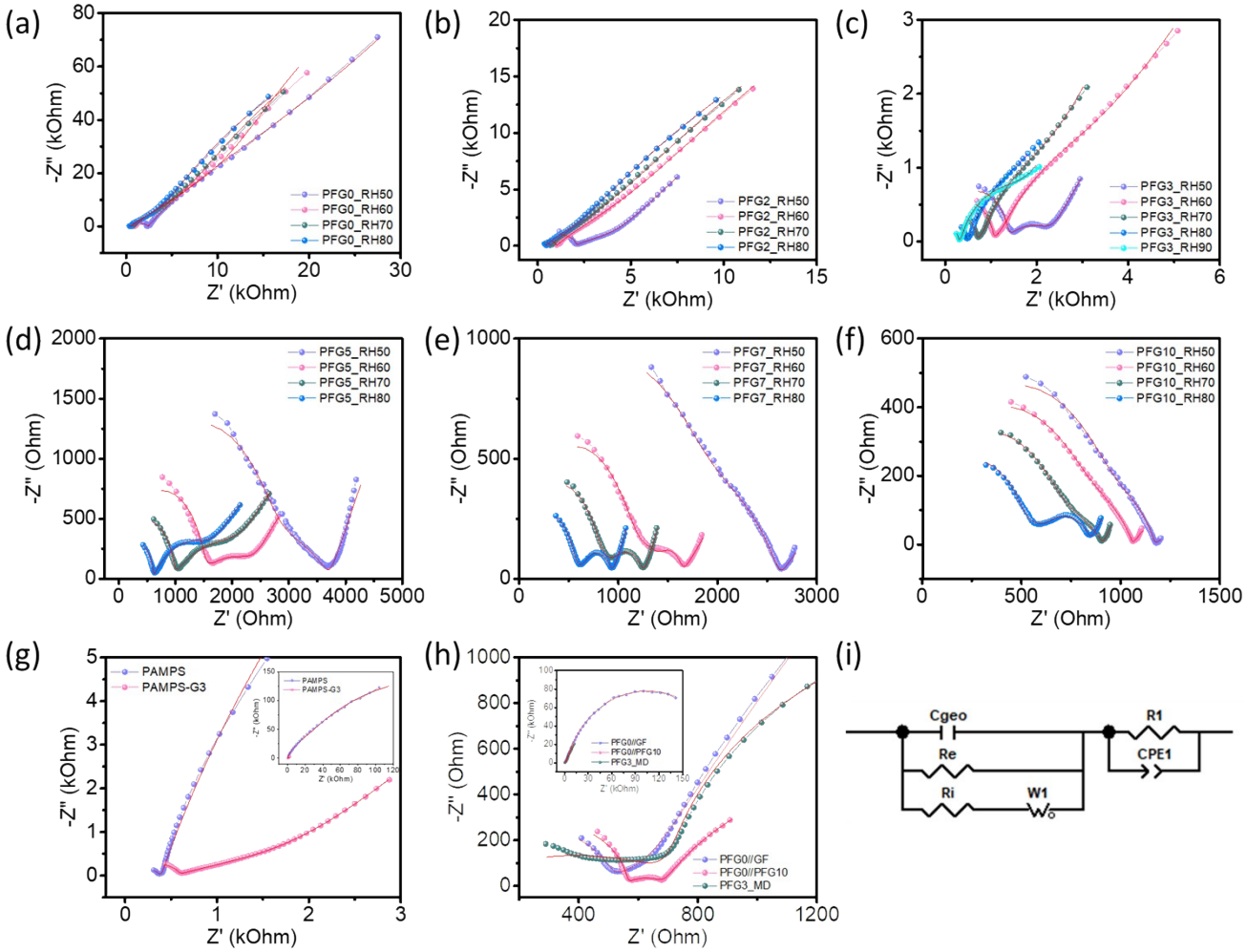

Figure S10. (a~f) Nyquist plot of PFGx (x = 0~10) films with various % RHs, (g) PAMPS and PG3 films at 80% RH (inset: Nyquist plot for full range), and (h) mTE films with different fabrication methods at 80% RH (inset: Nyquist plot for full range). (i) The equivalent circuit model for obtaining each element in the Table S4. The EIS was measured at an alternating voltage of 0.1 V under frequencies ranging from 1 MHz to 1 Hz. The fit line for all the spectra is presented as a red line in each Nyquist plot.

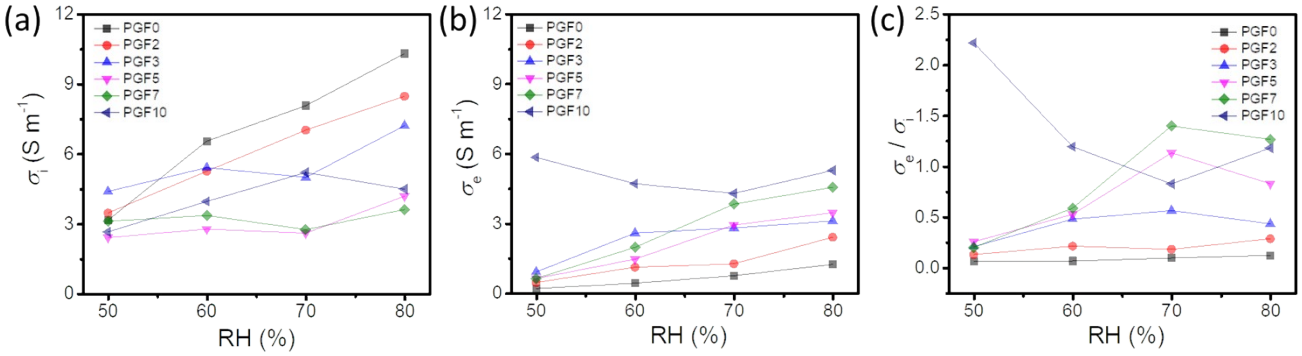

Figure S11. The (a) σ_i, (b) σ_e, and (c) σ_e/σ_i of the PFG films with various graphene flake concentrations at different % RH.

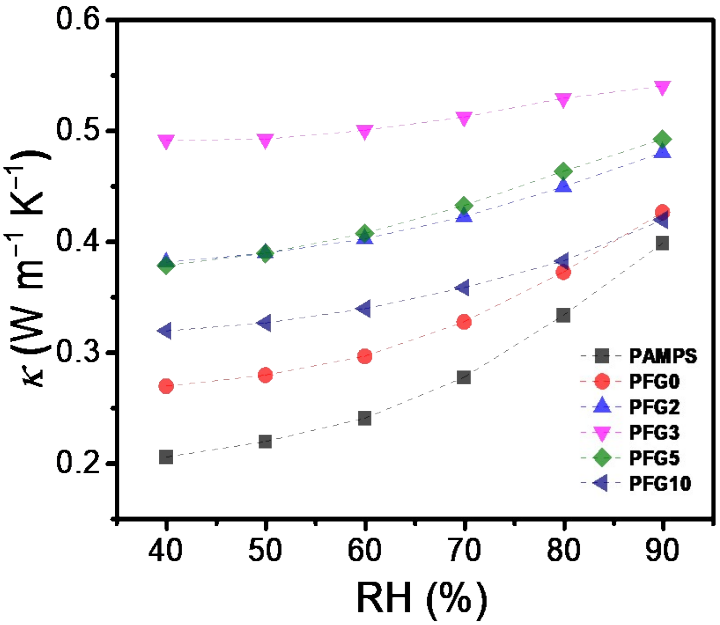

Figure S12. Thermal conductivities of PAMPS and PFG samples at various % RHs.

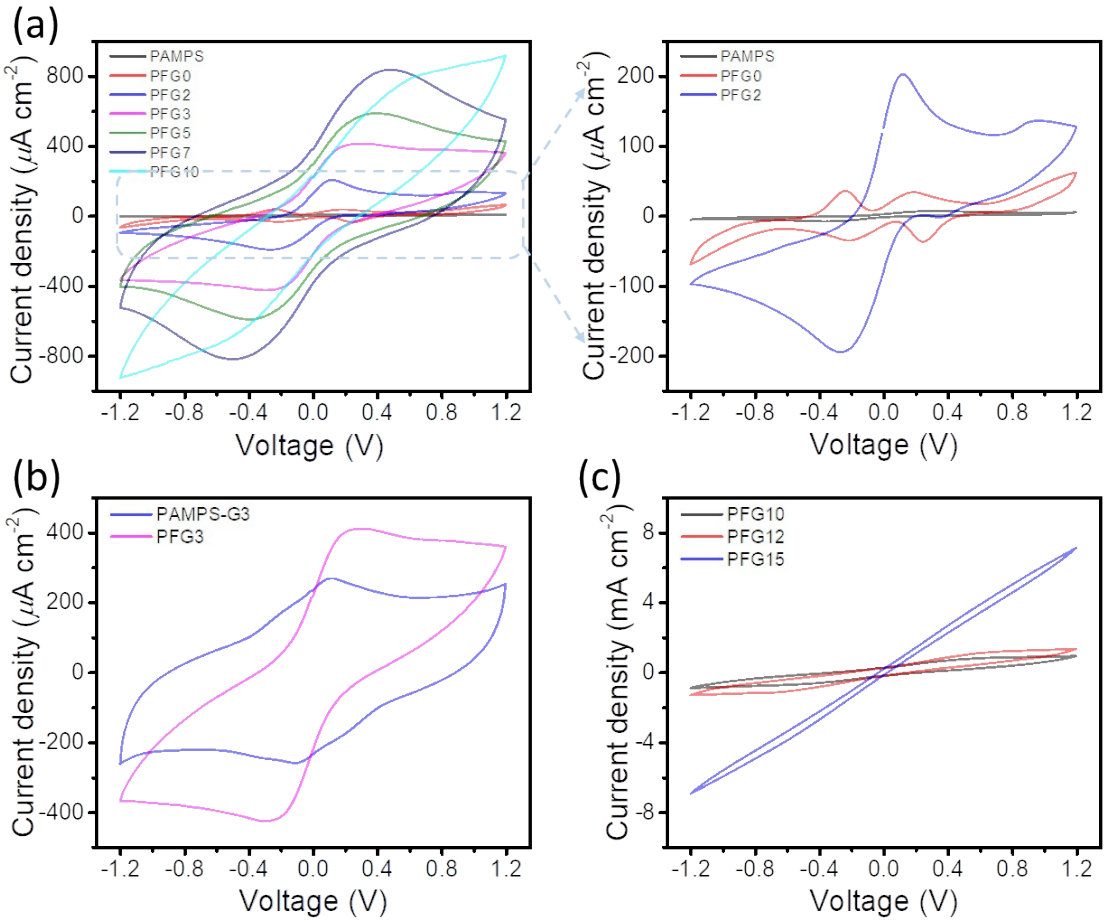

Figure S13. Cyclic voltammetry (CV) curves of (a) PAMPS and PFG0~10 films (inset: Magnified image for the CV curves of PAMPS, PFG0, and PFG2 films.), (b) PG3 and PFG3 films, and (c) PFG10~15 films at a scan rate of 50 mV s^{-1}.

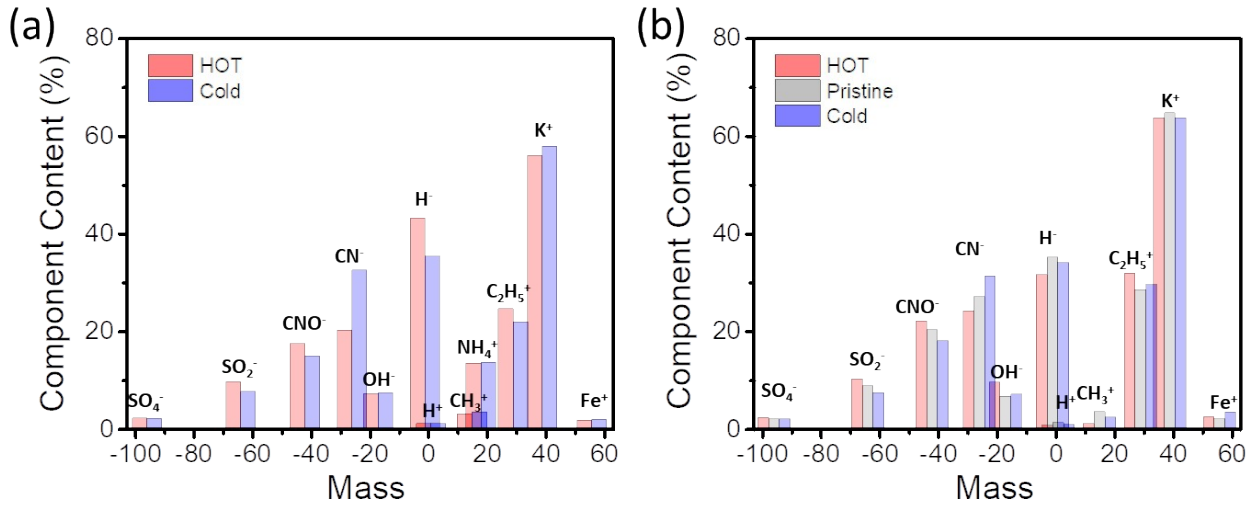

Figure S14. TOF-SIMS data in hot and cold regions (or pristine region) of the (a) PFG0 film and (b) PFG3 film for positive and negative ions at a ΔT of 5.3 K and 80% RH.

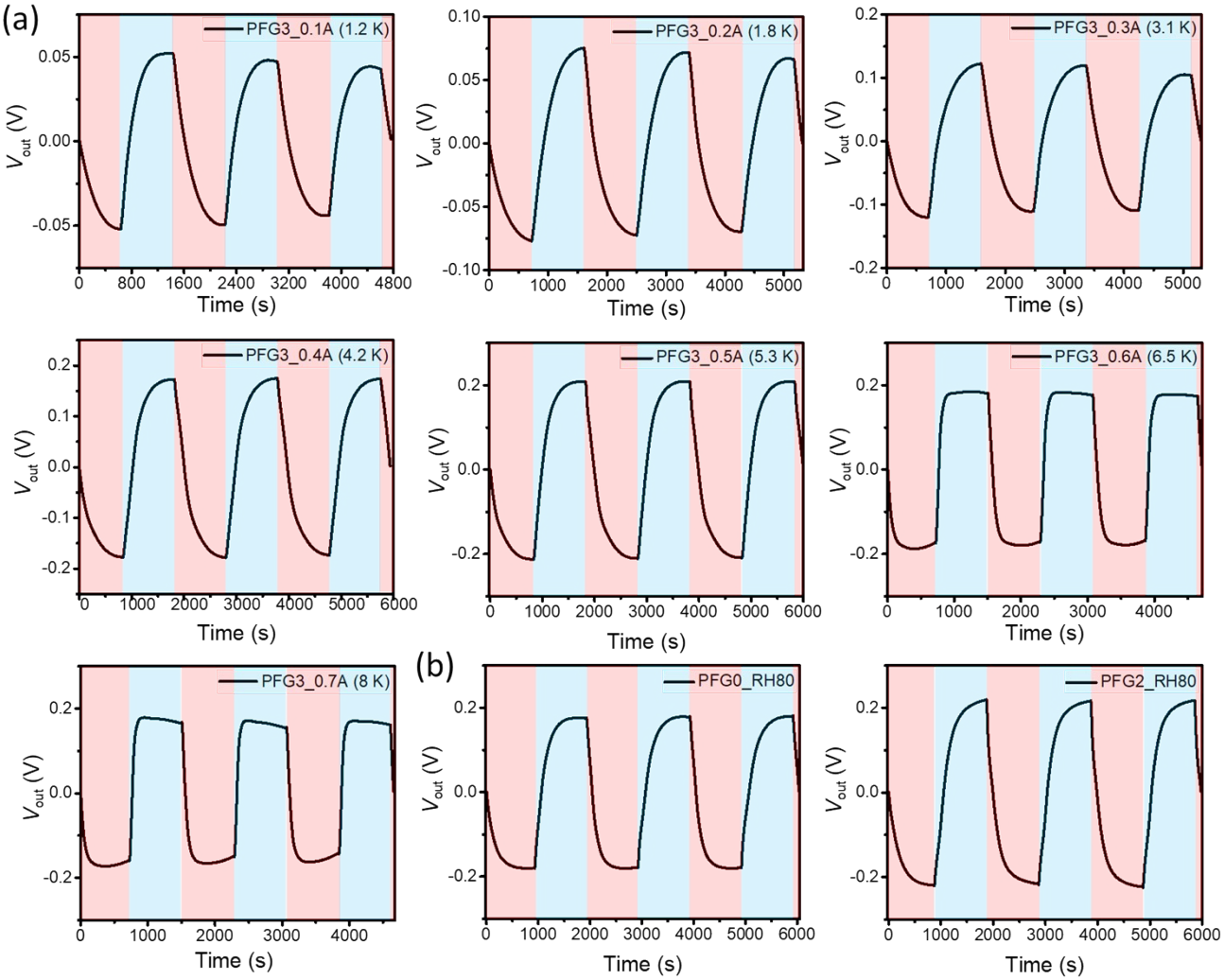

Figure S15. (a) V_{out} of the PFG3 film under 3 repeated heating–cooling cycles at different ΔT of 1.2, 1.8, 3.1, 4.2, 5.3, 6.5, and 8 K and 80% RH. (b) V_{out} of the PFG0 and PFG2 films under 3 repeated heating–cooling cycles at a ΔT of 5.3 K and 80% RH.

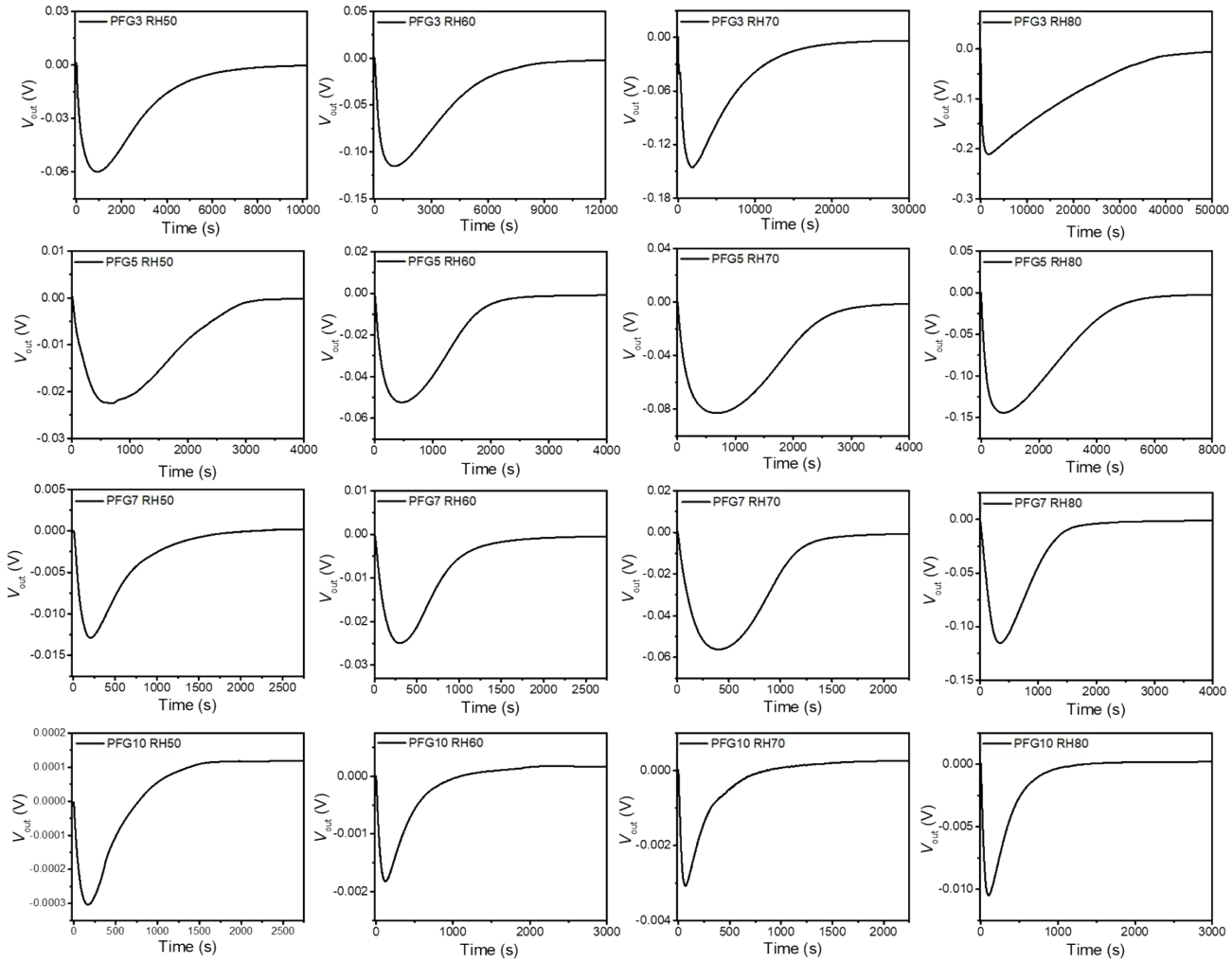

Figure S16. V_{out} of the PFG3~10 films at a long period under given ΔT of 5.3 K and 80% RH.

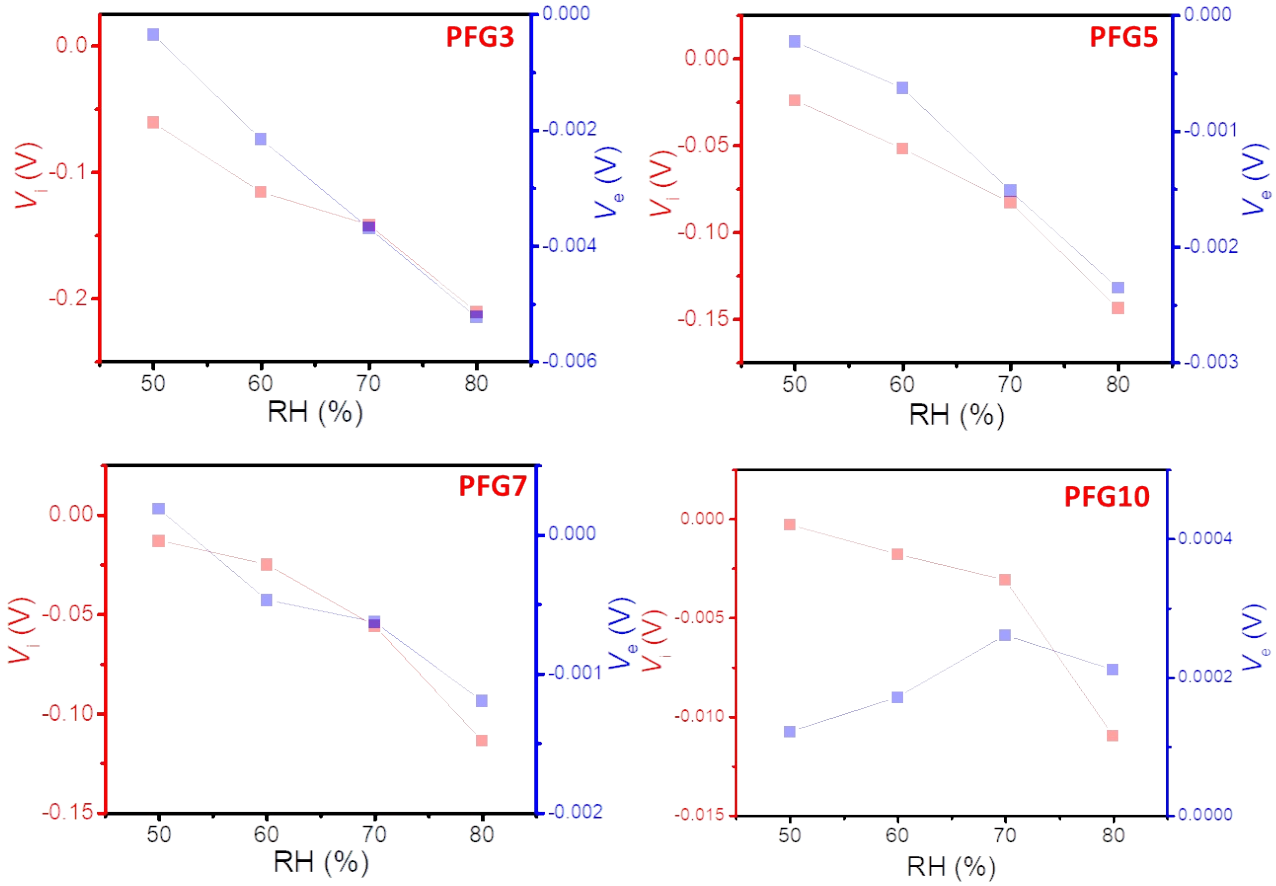

Figure S17. The V_i and V_e of the PFG3-10 films at various % RHs.

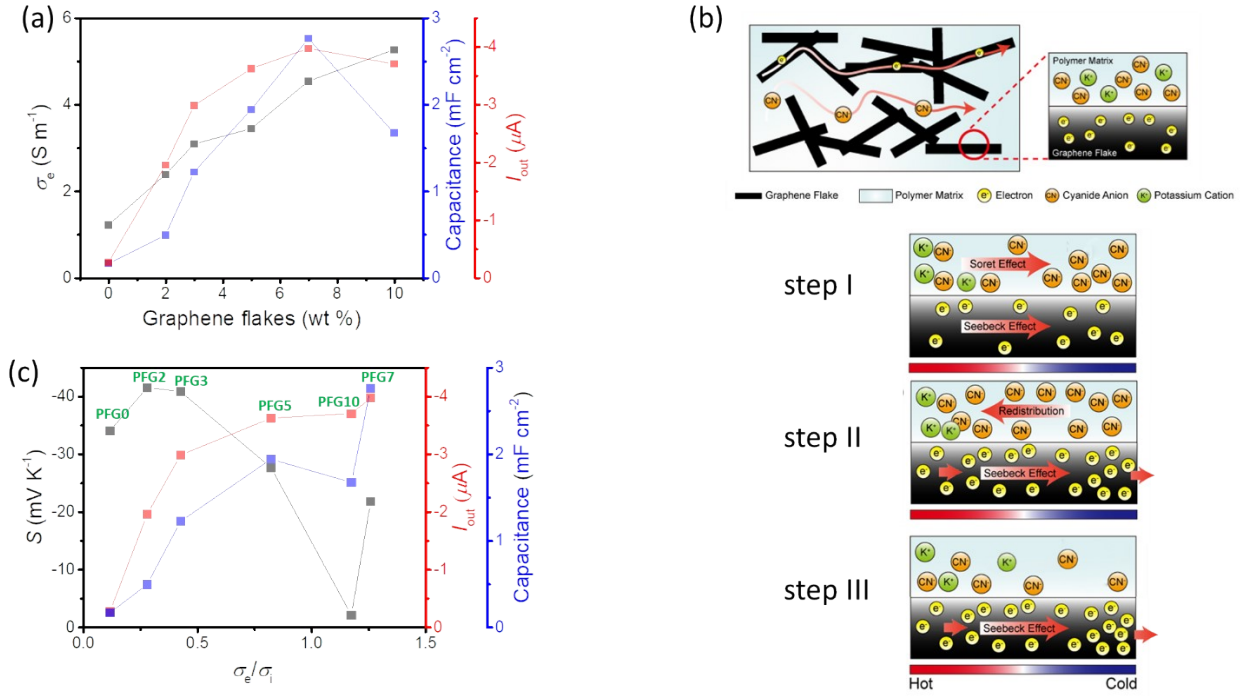

Figure S18. (a) σ_e, capacitance, I_{out} of the PFG films with various graphene flake concentrations and (b) Schematic drawing of the composton in PFG samples and the carrier transport at the step I ~ III for current evolution and decay during the TE conversion. (c) Correlation of S, I_{out} and capacitance of the PFG films according to σ_e/σ_i at a ΔT of 5.3 K and 80% RH.

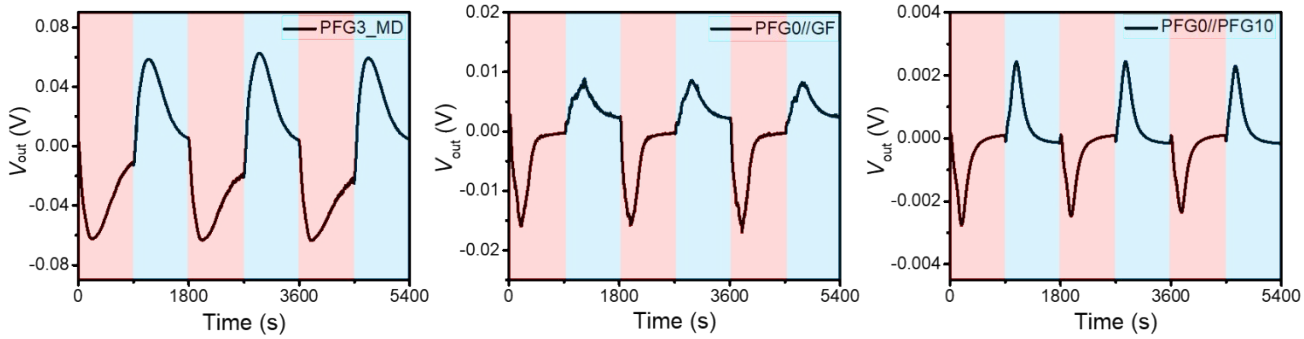

Figure S19. V_{out} of the PFG3_MD, PFG0//GF, and PFG0//PFG10 films under 3 repeated heating–cooling cycles at a ΔT of 5.3 K and 80% RH.

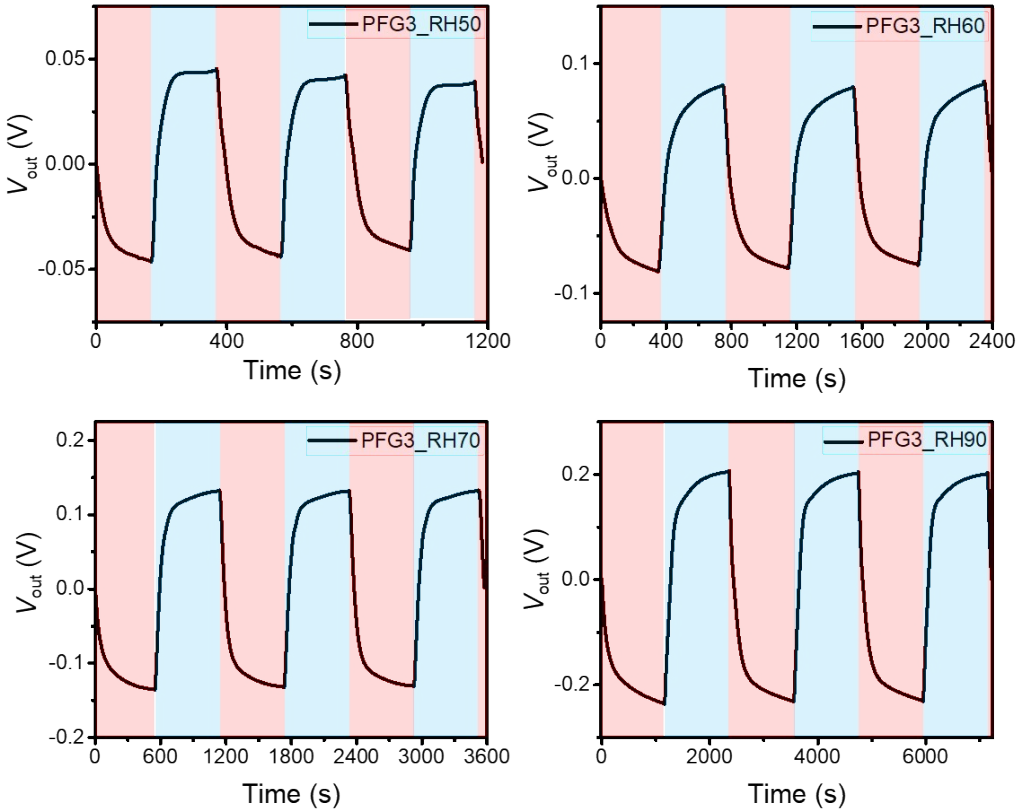

Figure S20. The V_{out} of the PFG3 film under 3 repeated heating–cooling cycles at a ΔT of 5.3 K and different % RHs.

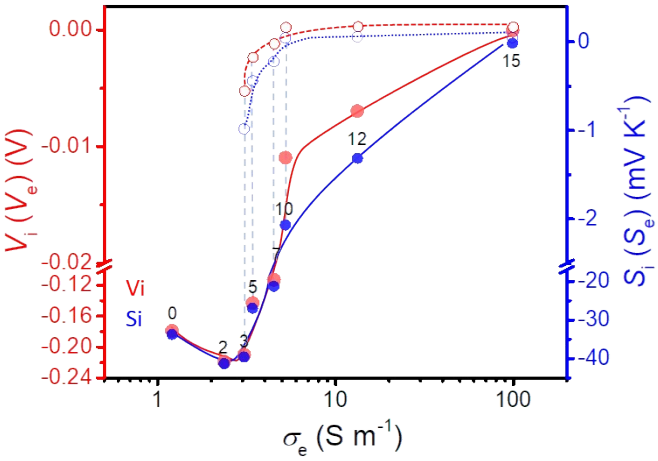

Figure S21. The V_i (red solid line), V_e (red dotted line), and S_i (blue solid line), and S_e (blue dotted line) of the PFG films with various graphene flake concentrations (as marked in the graph) according to σ_e.

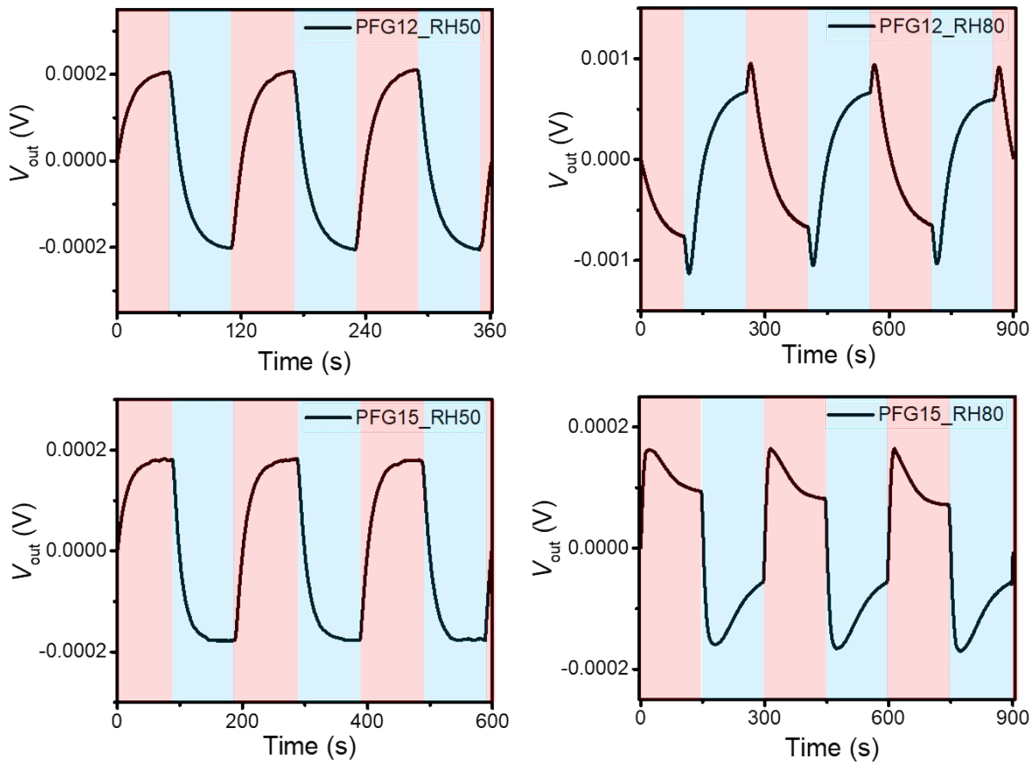

Figure S22. V_{out} of the PFG12 and PFG15 films under 3 repeated heating–cooling cycles at a ΔT of 5.3 K and 50, 80% RH.

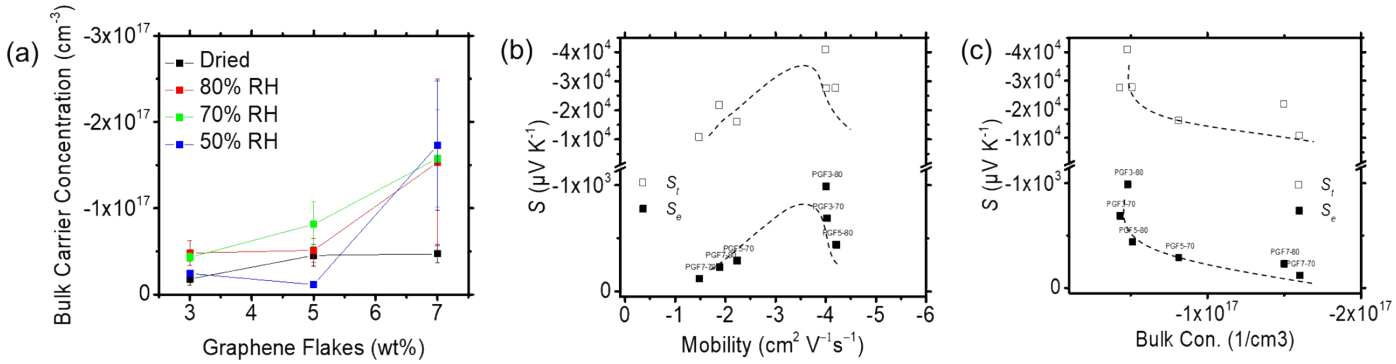

Figure S23. (a) Plot of *n* according to graphene contents from Hall measurement under dried (black), 50% RH (blue), 70% RH (green), and 80% RH (red). (b) Correlation of S_e (filled) and total *S* (empty) against mobility of PFG samples under 70 ~ 80%RH. (c) Correlation of S_e (filled) against n of PFG samples.

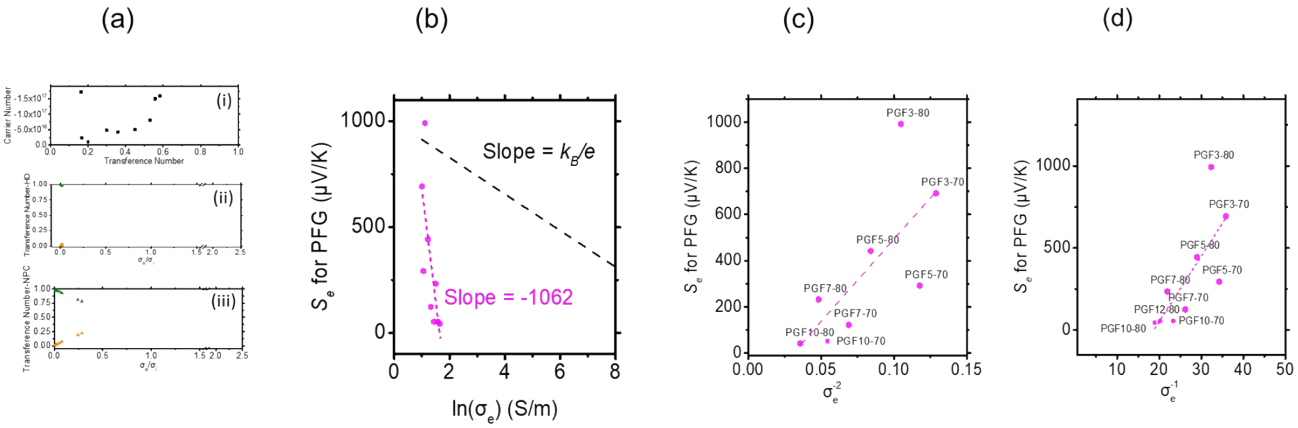

Figure S24. (a) Plot of (i) n according to te. (ii) t_i (green) and t_e (orange) of (ii) p-type highly doped PEDOT:PSS with PSSH (HDH) and (iii) n-type chloride doped PEDOT:PSS (NPC), according to σ_e/σ_i. (b) Plot of S_e against ln$\boldsymbol{\sigma}_e$ fitting with a slope of -1,062 (magenta) and calculated slope for k_b/e (black dashed line). (c) Plot of S_e against $\boldsymbol{\sigma}_e^{-2}$ (s = 0.5). (d) Plot of S_e against $\boldsymbol{\sigma}_e^{-1}$ (s = 1).

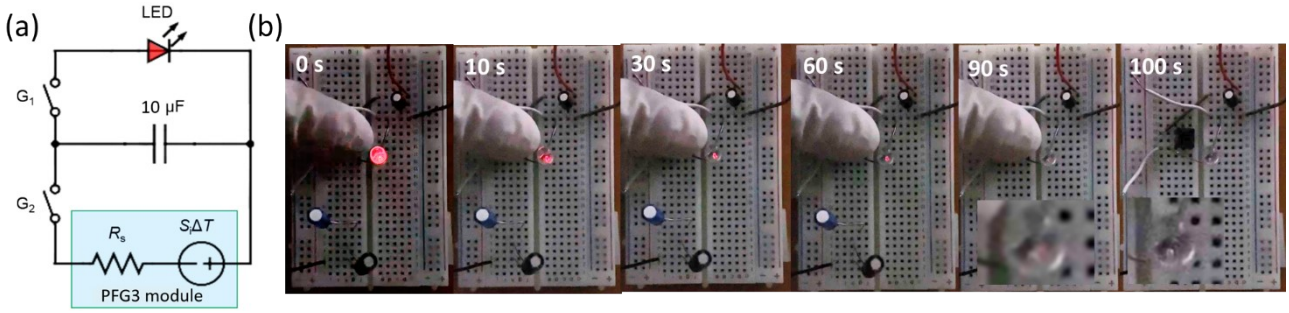

Figure S25. (a) Electrical circuit used for electrochemical energy storage and LED operation. (b) Photographs of LED turned on for 100 s (T_3 step described in Fig. 4b).

(a) PEDOT:Tos_RH50

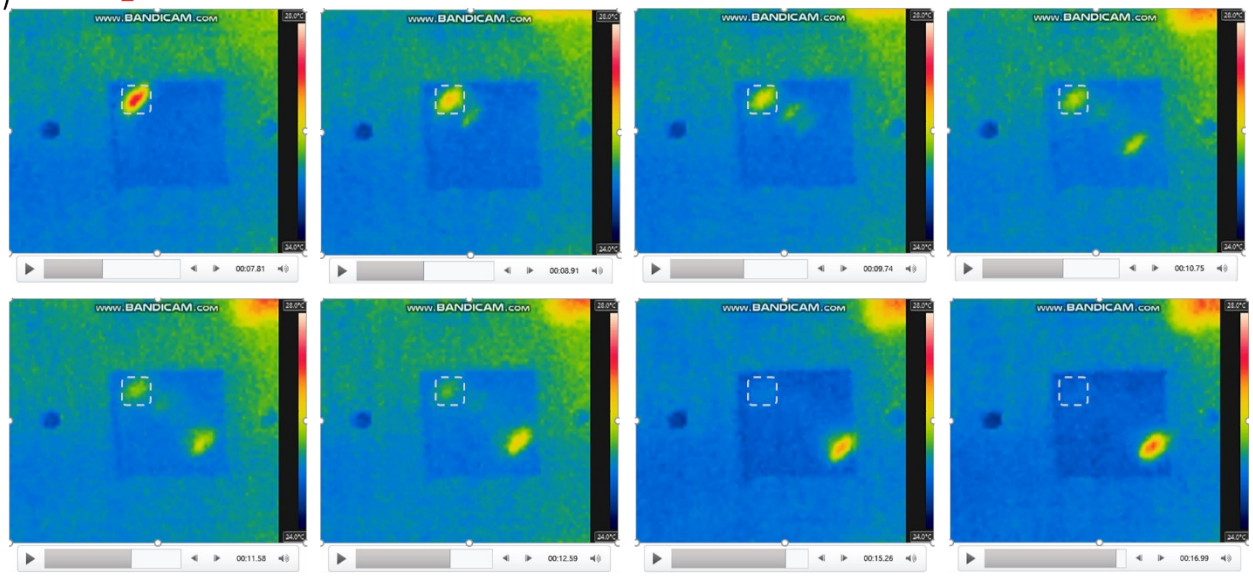

(b) PFG3_RH50

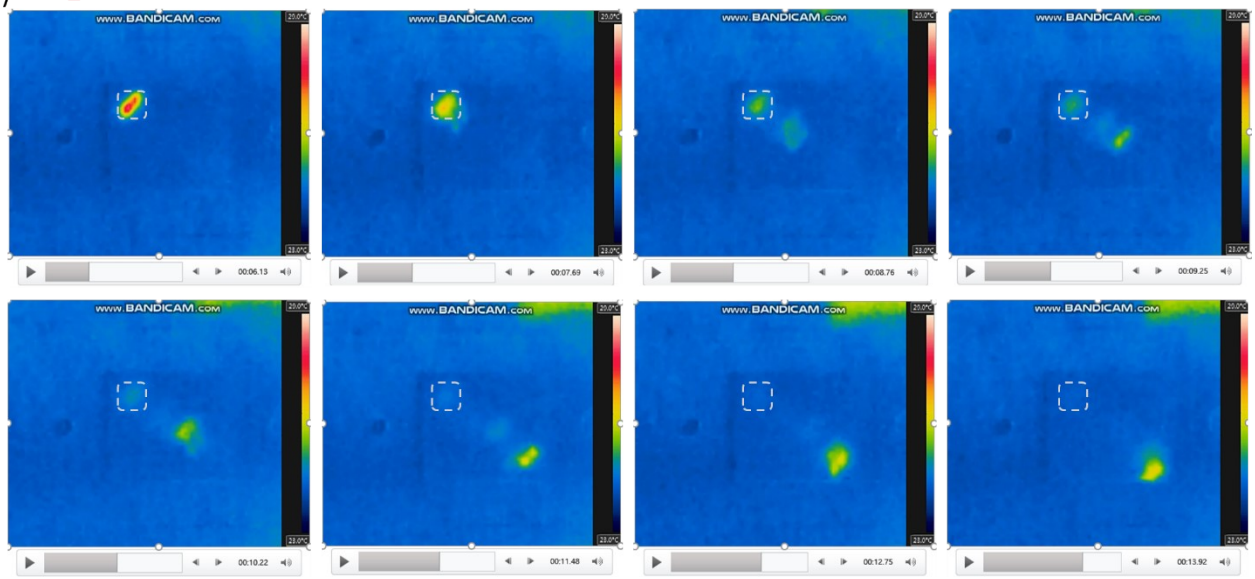

(c) PEDOT:Tos_RH80

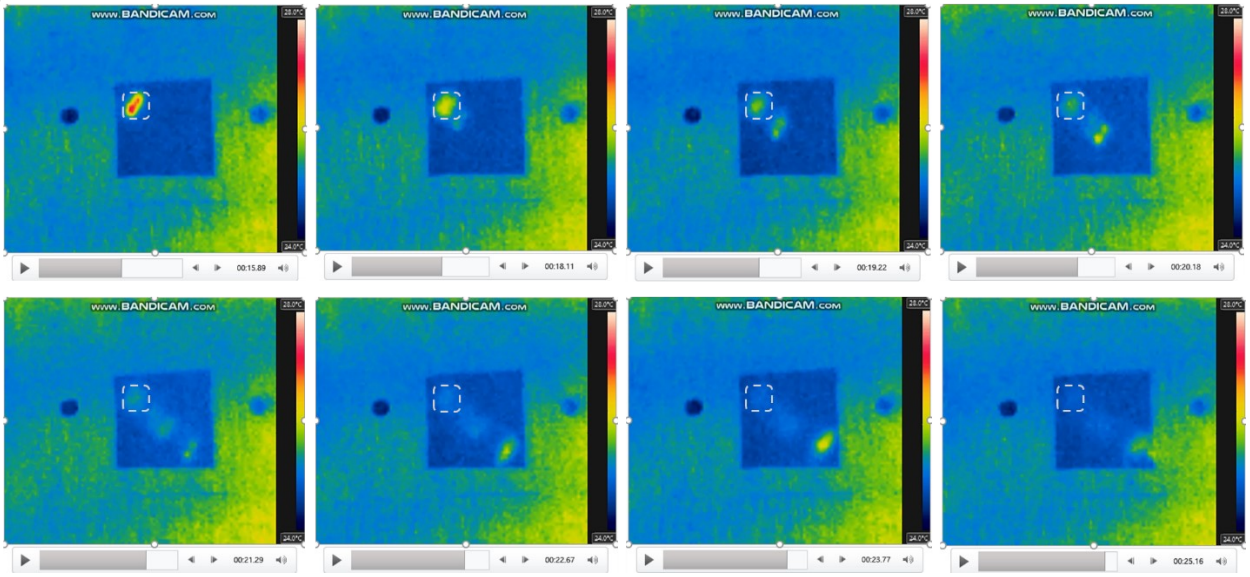

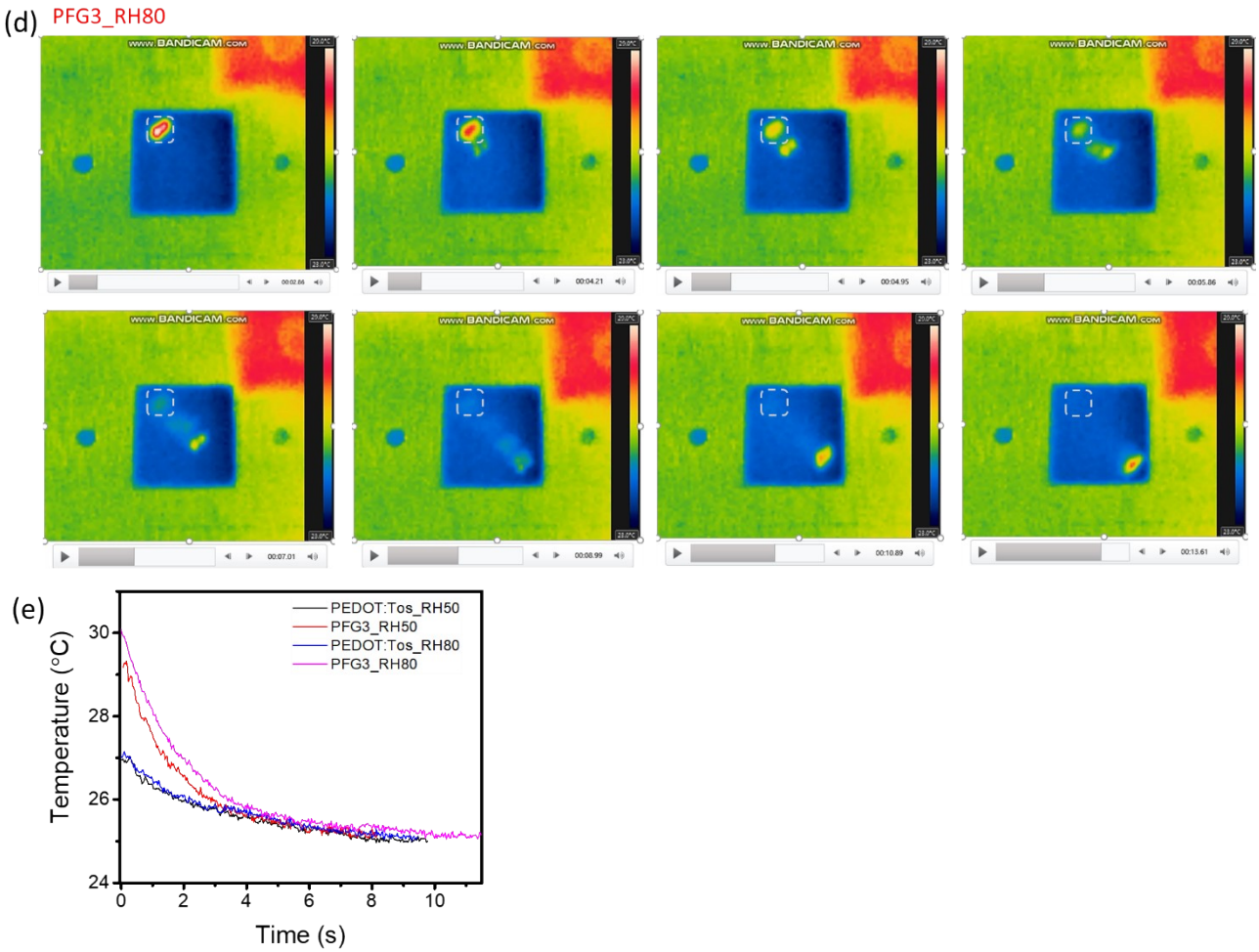

Figure S26. Thermal images of 2.5 × 2.5 cm^2 PEDOT:Tos (a, c) and PFG3 films (b, d) on the PET films at 50 and 80% RH, which were obtained using an IR camera. Each film was irradiated by a 1064 nm-NIR laser (*I*1064) with a laser power of 24.8 mW, and the laser moved in the diagonal direction. The dotted square is the point where the laser was first irradiated. (e) The temperature of irradiated points in the dotted square over time.

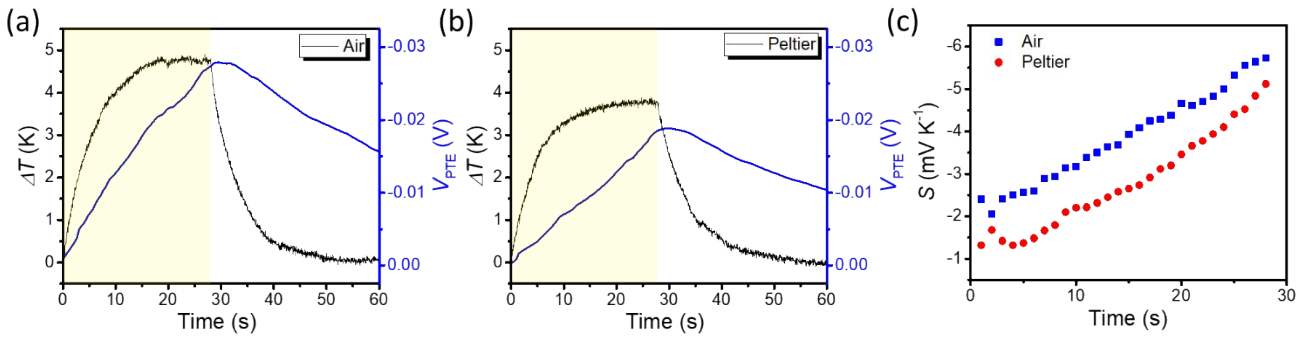

Figure S27. Temperature profile and V_{PTE} of the PFG3 film on the different substrate of (a) Air and (b) Peltier device where the *I*1064 with a laser power of 24.8 mW was irradiated. (c) The S_{PTE} profile of the PFG3 film on the different substrates during 30 s after the *I*1064 irradiation. Temperature profile was obtained using an IR camera. PTE measurements were performed at the RT and 80% RH.

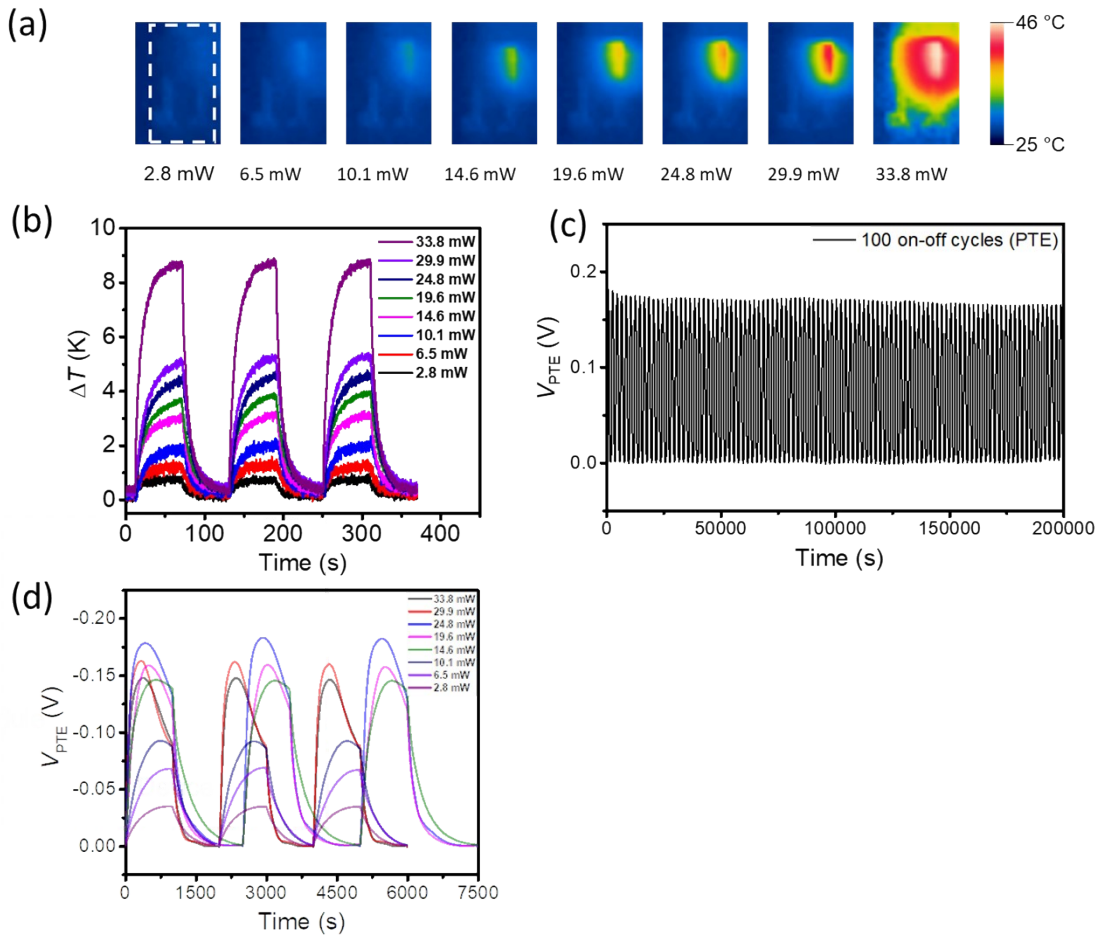

Figure S28. (a) Photographs of the PFG3 film heated using an NIR-laser (*I*1064) with various applied laser powers observed by an IR camera. (b) Temperature profile and (c) V_{PTE} of the PFG3 film under 100 repeated on–off cycles with a laser power of 24.8 mW at 80% RH. (d) V_{PTE} of the PFG3 film under 3 repeated on–off cycles with various applied laser powers and 80% RH

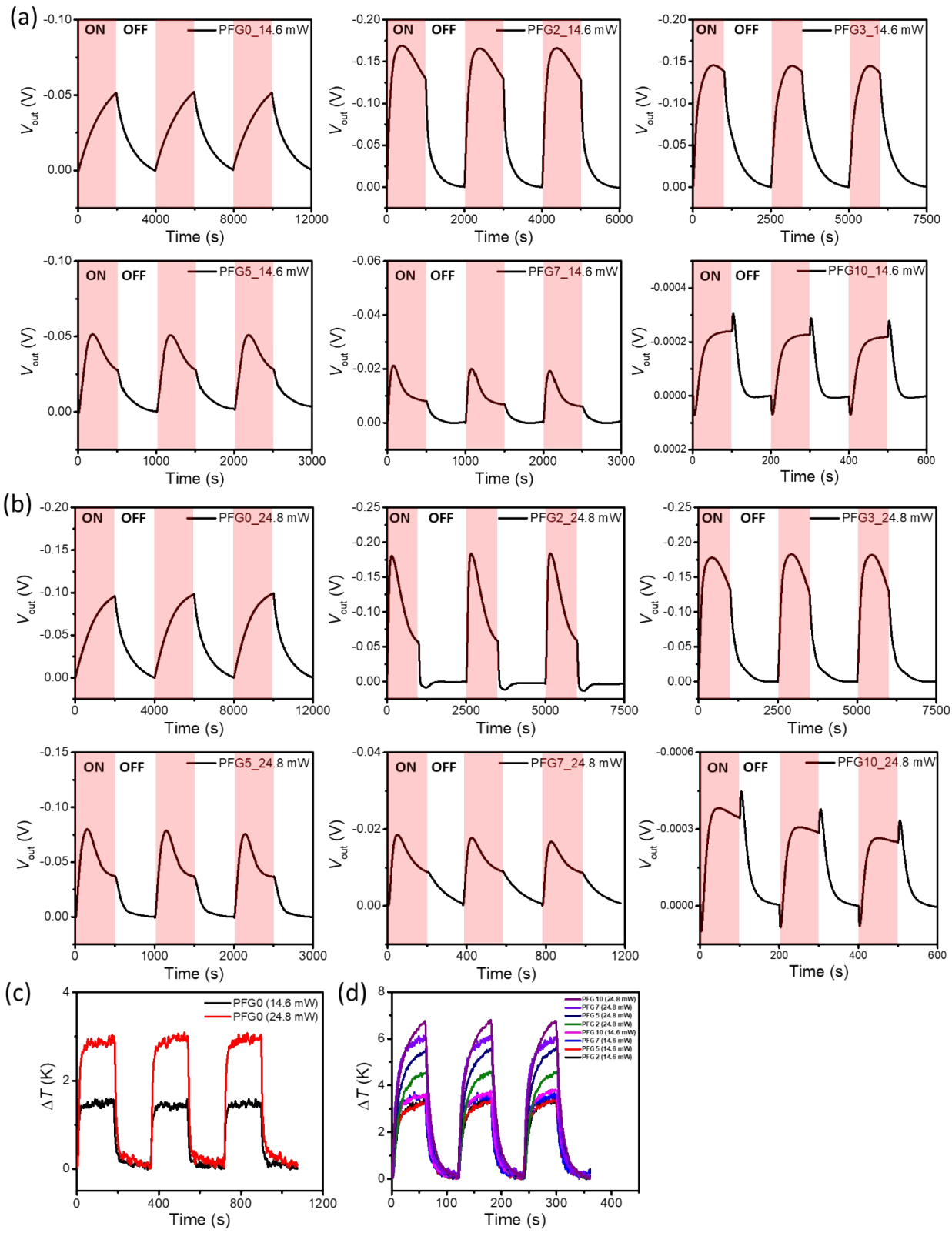

Figure S29. V_{PTE} of the PFG films under 3 repeated on–off cycles with laser powers of (a) 14.6 and (b) 24.8 mW at 80% RH. Temperature profile of (c) PFG0 film and (d) PFG2~10 films under 3 repeated on–off cycles with laser powers of 14.6 and 24.8 mW at 80% RH.

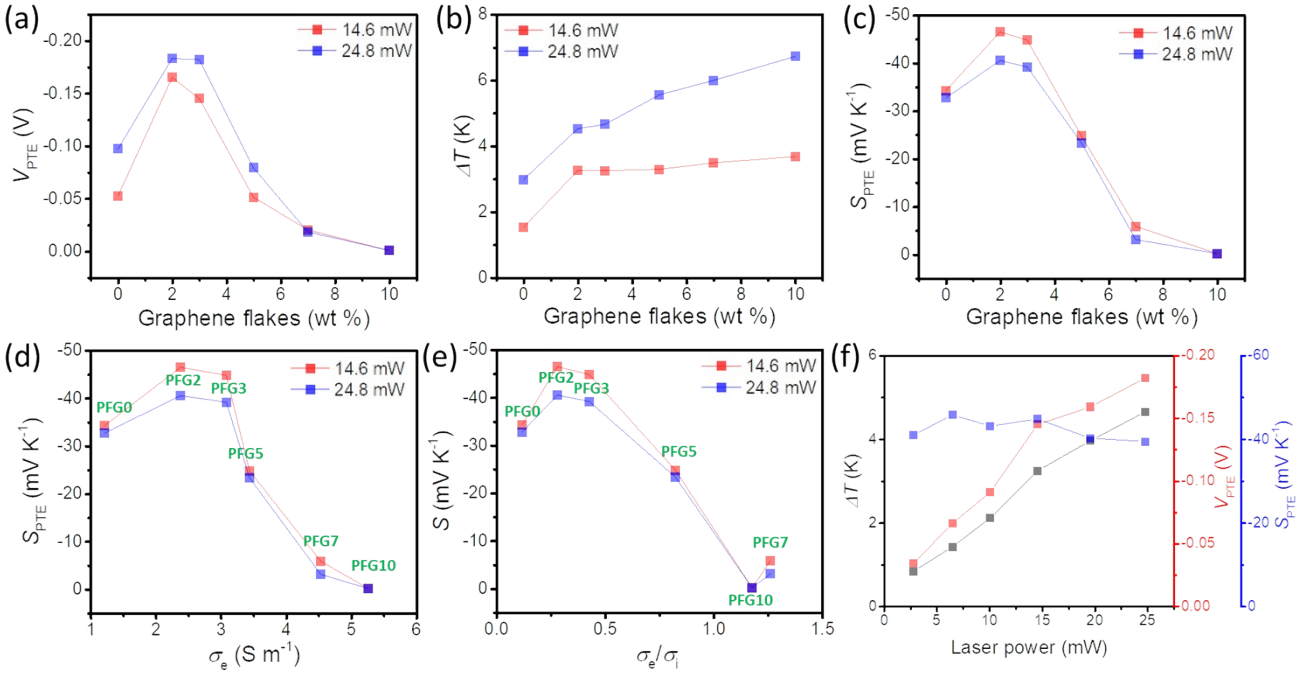

Figure S30. (a) V_{PTE}, (b) ΔT, and (c) S_{PTE} of the PFG films with various the graphene flake concentrations at laser powers of 14.6 and 24.8 mW and 80% RH. S_{PTE} of the PFG films according to (d) σ_e and (e) σ_e/σ_i with laser powers of 14.6, 24.8 mW and 80% RH. (f) The ΔT, V_{PTE}, and S_{PTE} of PFG3 film with various applied laser powers at 80% RH.

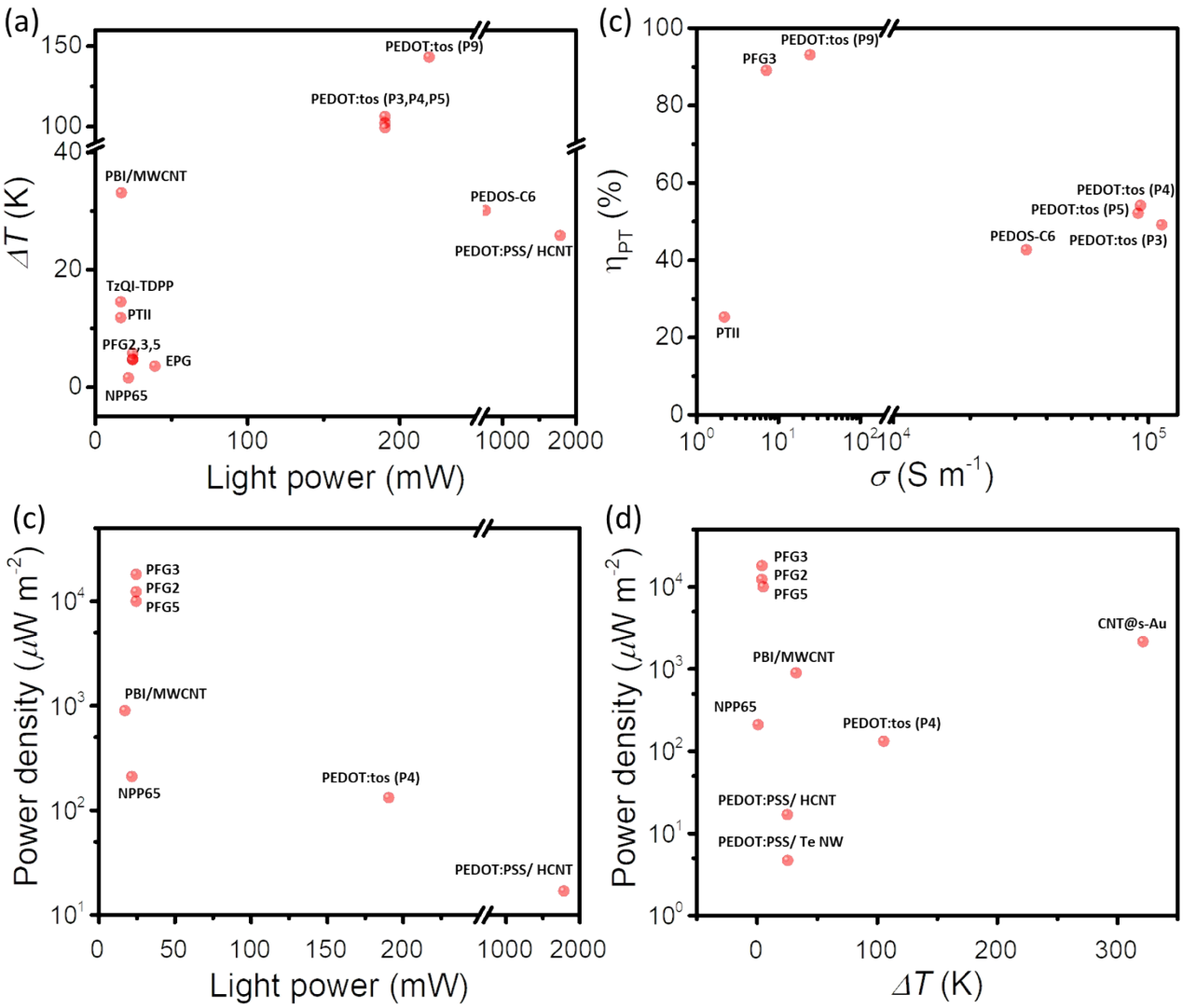

Figure S31. (a) The ΔT generated by different laser powers, (b) η_{PT} according to the σ, and the power density with different (c) laser powers and (d) ΔT at various reported PTE materials (Table S7).

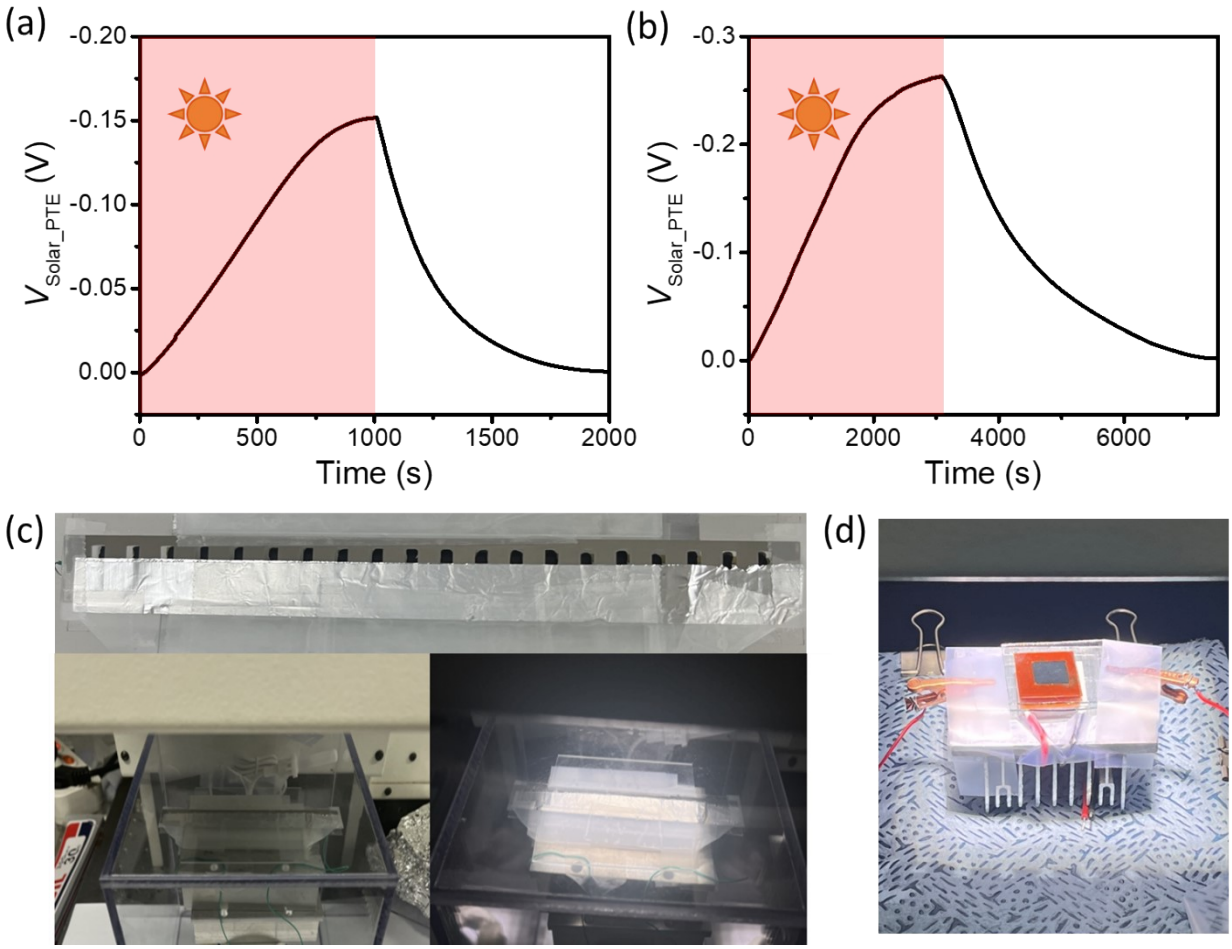

Figure S32. $V_{solar\text{-}PTE}$ of the (a) planarly and (b) vertically structured PFG3 film (thickness: 3 mm) under artificial sunlight with 1 sun power (100 mW cm^{-2}). (c) Photographs of a PTE module with 20 PFG3 legs and the solar-PTE measurement of a PFG3 module at 80% RH using artificial sunlight supplied by a solar simulator. The remaining area except for the local area (2 × 2 mm^2) at the end of each leg was covered with an aluminum foil attached stainless mask. (d) Photograph of a vertically structured PFG3 film on a heat sink under artificial sunlight.

Supplementary video

Supporting Video 1.

Supplemental references

1. S. Riaz, N. Fatima, A. Rasheed, M. Riaz, F. Anwar and Y. Khatoon, *International Journal of Biomaterials*, 2018, 2018, 1963024.
2. T. Yamashita and P. Hayes, *Applied Surface Science*, 2008, 254, 2441-2449.
3. B. Kim, M. Han and E. Kim, *Journal of Materials Chemistry A*, 2019, 7, 2066-2074.
4. D. Zhao, A. Würger and X. Crispin, *Journal of Energy Chemistry*, 2021, 61, 88-103.
5. C. Cho, B. Kim, S. Park and E. Kim, *Energy & Environmental Science*, 2022, 15, 2049-2060.
6. B. Kim, J. U. Hwang and E. Kim, *Energy & Environmental Science*, 2020, 13, 859-867.
7. B. Kim, J. Na, H. Lim, Y. Kim, J. Kim and E. Kim, *Advanced Functional Materials*, 2019, 29, 1807549.
8. H. Cheng, S. Yue, Q. Le, Q. Qian and J. Ouyang, *Journal of Materials Chemistry A*, 2021, 9, 13588-13596.
9. Y. T. Malik, Z. A. Akbar, J. Y. Seo, S. Cho, S.-Y. Jang and J.-W. Jeon, *Advanced Energy Materials*, 2022, 12, 2103070.
10. Z. Liu, H. Cheng, Q. Le, R. Chen, J. Li and J. Ouyang, *Advanced Energy Materials*, 2022, 12, 2200858.
11. X. He, H. Cheng, S. Yue and J. Ouyang, *Journal of Materials Chemistry A*, 2020, 8, 10813-10821.
12. C. Zhou, Y. K. Lee, Y. Yu, S. Byun, Z.-Z. Luo, H. Lee, B. Ge, Y.-L. Lee, X. Chen, J. Y. Lee, O. Cojocaru-Mirédin, H. Chang, J. Im, S.-P. Cho, M. Wuttig, V. P. Dravid, M. G. Kanatzidis and I. Chung, *Nature Materials*, 2021, 20, 1378-1384.
13. B. Cai, H.-L. Zhuang, Q. Cao, H. Hu, J. Dong, Asfandiyar and J.-F. Li, *ACS Applied Materials & Interfaces*, 2020, 12, 16426-16435.
14. G. Tan, F. Shi, S. Hao, L.-D. Zhao, H. Chi, X. Zhang, C. Uher, C. Wolverton, V. P. Dravid and M. G. Kanatzidis, *Nature Communications*, 2016, 7, 12167.
15. H. J. Wu, L. D. Zhao, F. S. Zheng, D. Wu, Y. L. Pei, X. Tong, M. G. Kanatzidis and J. Q. He, *Nature Communications*, 2014, 5, 4515.
16. L.-D. Zhao, S.-H. Lo, Y. Zhang, H. Sun, G. Tan, C. Uher, C. Wolverton, V. P. Dravid and M. G. Kanatzidis, *Nature*, 2014, 508, 373-377.
17. B. Zhong, Y. Zhang, W. Li, Z. Chen, J. Cui, W. Li, Y. Xie, Q. Hao and Q. He, *Applied Physics Letters*, 2014, 105, 123902-123902.
18. K. Zhao, E. Eikeland, D. He, W. Qiu, Z. Jin, Q. Song, T.-r. Wei, P. Qiu, J. Liu, J. He, B. B. Iversen, J. He, L. Chen and X. Shi, *Joule*, 2021, 5, 1183-1195.
19. L. Yang, M. P. Gordon, A. K. Menon, A. Bruefach, K. Haas, M. C. Scott, R. S. Prasher and J. J. Urban, *Science Advances*, 2021, 7, eabe6000.
20. C. Xiong, F. Shi, H. Wang, J. Cai, S. Zhao, X. Tan, H. Hu, G. Liu, J. G. Noudem and J. Jiang, *ACS Applied Materials & Interfaces*, 2021, 13, 15429-15436.
21. L. Hu, H. Wu, T. Zhu, C. Fu, J. He, P. Ying and X. Zhao, *Advanced Energy Materials*, 2015, 5, 1500411.
22. Y. Liu, X. Lan, J. Xu, W. Zhou, C. Liu, C. Liu, P. Liu, M. Li and F. Jiang, *ACS Applied Materials & Interfaces*, 2021, 13, 43155-43162.
23. X. Li, M. Sheng, J. Liang, J. Zheng, Y. Zheng, S. Wang, Q. Li, L.-D. Zhao, Y. Deng and Y. Wang, *Advanced Functional Materials*, 2023, 33, 2303352.
24. J. Park and Y. G. Jeong, *ACS Applied Electronic Materials*, 2022, 4, 386-393.
25. X.-z. Jin, H. Li, Y. Wang, Z.-y. Yang, X.-d. Qi, J.-h. Yang and Y. Wang, *ACS Applied Materials & Interfaces*, 2022, 14, 27083-27095.
26. B. Kim, H. Shin, T. Park, H. Lim and E. Kim, *Advanced Materials*, 2013, 25, 5483-5489.
27. T. Hasegawa, M. Ashizawa, Y. Hayashi, S. Kawauchi, H. Masunaga, T. Hikima, T. Manaka and H. Matsumoto, *ACS Applied Polymer Materials*, 2019, 1, 542-551.
28. B. Kim, C. Cho, M. Han, A.-J. Attias and E. Kim, *Advanced Functional Materials*, 2021, 31, 2105297.